


## RESEARCH ARTICLE

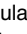
Mapping *Rora* expression in resting and activated CD4+ T cells

Liora Haim-Vilmovsky<sup>1,2</sup>, Johan Henriksson<sup>1,2</sup>, Jennifer A. Walker<sup>3</sup>, Zhichao Miao<sup>1,2</sup>, Eviatar Natan<sup>1</sup>, Gozde Kar<sup>1,2</sup>, Simon Clare<sup>2</sup>, Jillian L. Barlow<sup>3</sup>, Evelina Charidemou<sup>4</sup>, Lira Mamanova<sup>2</sup>, Xi Chen<sup>2</sup>, Valentina Proserpio<sup>1,2</sup>, Jhuma Pramanik<sup>2</sup>, Steven Woodhouse<sup>5,6</sup>, Anna V. Protasio<sup>2</sup>, Mirjana Efremova<sup>2</sup>, Julian L. Griffin<sup>4,7</sup>, Matt Berriman<sup>2</sup>, Gordon Dougan<sup>2</sup>, Jasmin Fisher<sup>8</sup>, John C. Marioni<sup>1,2,9</sup>, Andrew N. J. McKenzie<sup>3</sup>, Sarah A. Teichmann<sup>1,2,10</sup>

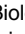
**1** EMBL-European Bioinformatics Institute, Wellcome Genome Campus, Hinxton, Cambridge, United Kingdom, **2** Wellcome Sanger Institute, Wellcome Genome Campus, Hinxton, Cambridge, United Kingdom, **3** MRC Laboratory of Molecular Biology, Cambridge Biomedical Campus, Cambridge, United Kingdom, **4** Department of Biochemistry, University of Cambridge, Cambridge, United Kingdom, **5** Department of Haematology, Cambridge Institute for Medical Research, University of Cambridge, Cambridge, United Kingdom, **6** Wellcome Trust—Medical Research Council Cambridge Stem Cell Institute, University of Cambridge, Cambridge, United Kingdom, **7** Department of Metabolism, Digestion and Reproduction, Biomolecular Medicine, Imperial College London, London, United Kingdom, **8** Microsoft Research, Cambridge, United Kingdom, **9** Cancer Research UK Cambridge Institute, University of Cambridge, Cambridge, United Kingdom, **10** Theory of Condensed Matter, Cavendish Laboratory, Cambridge, United Kingdom

 These authors contributed equally to this work.


 Current address: Laboratory for Molecular Infection Medicine Sweden (MIMS), Umeå University, Umeå, Sweden

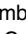
 Current address: Department of Molecular Biology, Umeå University, Umeå, Sweden

 Current address: The Aleph Lab, Oxford, United Kingdom

 Current address: Translational Medicine, Research and Early Development, Oncology R&D, AstraZeneca, Cambridge, United Kingdom


 Current address: Department of Biology, University of York, Wentworth Way, York, United Kingdom

 Current address: Department of Biology, South University of Science and Technology of China, Shenzhen, China

 Current address: IIGM Foundation—Italian Institute for Genomic Medicine, Candiolo, Torino, Italy

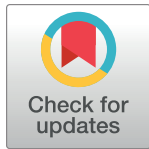
 Current address: Candiolo Cancer Institute, FPO-IRCCS, Candiolo, Torino, Italy

 Current address: Department of Pathology, University of Cambridge, Cambridge, United Kingdom

 Current address: Department of Genetics, University of Pennsylvania, Philadelphia, Pennsylvania, United States of America

 Current address: UCL Cancer Institute, University College London, London, United Kingdom

\* [st9@sanger.ac.uk](mailto:st9@sanger.ac.uk)



## OPEN ACCESS

**Citation:** Haim-Vilmovsky L, Henriksson J, Walker JA, Miao Z, Natan E, Kar G, et al. (2021) Mapping *Rora* expression in resting and activated CD4+ T cells. PLoS ONE 16(5): e0251233. <https://doi.org/10.1371/journal.pone.0251233>

**Editor:** Scott N. Mueller, The University of Melbourne, AUSTRALIA

**Received:** April 1, 2021

**Accepted:** April 22, 2021

**Published:** May 18, 2021

**Copyright:** © 2021 Haim-Vilmovsky et al. This is an open access article distributed under the terms of the [Creative Commons Attribution License](https://creativecommons.org/licenses/by/4.0/), which permits unrestricted use, distribution, and reproduction in any medium, provided the original author and source are credited.

**Data Availability Statement:** The sequencing data has been deposited at ArrayExpress (E-MTAB-7694, E-MTAB-8000, E-MTAB-8001, E-MTAB-8003), and the image data at Zenodo (<https://doi.org/10.5281/zenodo.2554078>). The R code used for the analysis is available on GitHub (<https://github.com/mahogny/liorarora>).

**Funding:** This study was supported by EMBO in the form of a grant awarded to LHV (ALTF 698-2012), Directorate-General for Research and Innovation in the form of a grant awarded to LHV (FP7-PEOPLE-2010-IEF, ThPLAST 274192), an

## Abstract

The transcription factor *Rora* has been shown to be important for the development of ILC2 and the regulation of ILC3, macrophages and Treg cells. Here we investigate the role of *Rora* across CD4+ T cells in general, but with an emphasis on Th2 cells, both *in vitro* as well as in the context of several *in vivo* type 2 infection models. We dissect the function of *Rora* using overexpression and a CD4-conditional *Rora*-knockout mouse, as well as a RORA-reporter mouse. We establish the importance of *Rora* in CD4+ T cells for controlling lung inflammation induced by *Nippostrongylus brasiliensis* infection, and have measured the effect on downstream genes using RNA-seq. Using a systematic stimulation screen of CD4+ T cells, coupled with RNA-seq, we identify upstream regulators of *Rora*, most importantly

EMBL Interdisciplinary Postdoctoral fellowship, supported by H2020 Marie Skłodowska Curie Actions and awarded to LHV, the Swedish Research Council in the form of a grant awarded to JH (#2016-06598), the European Research Council in the form of a grant awarded to SAT (ThDEFINE), FUV - Fondazione Umberto Veronesi in the form of funds awarded VP, UK Medical Research Council in the form of a grant awarded to JW and ANJM (U105178805), Wellcome Trust in the form of a grant awarded to JW and ANJM (100963/Z/13/Z) and a Single Cell Gene Expression Atlas grant awarded to ZM (108437/Z/15/Z), and the Open Targets Grant awarded to ZM (OTAR2067). Wellcome Sanger Institute core facilities are supported by a grant (WT206194). Microsoft Research Cambridge, a subsidiary of Microsoft, provided support in the form of a salary for JF. The specific roles of these authors are articulated in the 'author contributions' section. The funders had no role in the study design, data collection and analysis, decision to publish, or preparation of the manuscript.

**Competing interests:** The authors have read the journal's policy and have the following competing interests: JF was an employee of Microsoft Research Cambridge at the time the study was conducted, but is no longer an employee of the company. EN is an employee of Aleph Labs, but was not employed by the company at the time the study was conducted. GK is an employee of AstraZeneca, but was not employed by the company at the time the study was conducted. This does not alter our adherence to PLOS ONE policies on sharing data and materials. There are no patents, products in development or marketed products associated with this research to declare.

IL-33 and CCL7. Our data suggest that *Rora* is a negative regulator of the immune system, possibly through several downstream pathways, and is under control of the local microenvironment.

## Introduction

Type 2 response is driven by a broad range of stimuli including helminths, allergens, specific bacterial and viral infections, and endogenous host molecules [1]. This reaction is characterized by a cellular repertoire which include the innate lymphoid cells type 2 (ILC2) [2, 3] and adaptive T helper 2 (Th2) which are known to express transcription factor GATA-binding protein 3 (GATA-3). Those cells secrete distinct cytokines including interleukin-4 (IL-4), IL-5, and IL-13, driving eosinophil recruitment and immunoglobulin production.

Retinoic acid receptor-related orphan receptor alpha (*Rora*), is a nuclear receptor that functions as a ligand-dependent transcription factor [4–6], and is known to regulate functions in immunity in addition to other roles in development, circadian rhythm and metabolism [7]. *Rora* was found to play a critical role in the development of ILC2 [8, 9] and for cytokine production in ILC3 [10]. In the liver, it controls inflammation by promoting the macrophage M2 polarization [11]. Together with *Rorc*, it influences the development of Th17 [12]. Recently it was shown to have an important role in skin Tregs, where it is required for proper regulation of the immune response in atopic dermatitis. In this study, the deletion of *Rora* in Tregs resulted in exaggerated type 2 allergic skin inflammation, increased expression of *Il-10*, *Ahr* and *Il-4*, while *Tnfrsf25* expression was reduced [13].

Given this previous literature, we hypothesised that *Rora* might be involved in regulating an inflammatory response via CD4<sup>+</sup> T cells more widely. To investigate this we assessed the function of *Rora* in four different infection models involving, but not limited to, type 2 immunity (Fig 1).

By employing bulk RNA sequencing (RNA-seq), single cell RNA-seq (scRNA-seq) and mass spectrometry (MS) analysis of T helper cells, we have investigated the role played by *Rora* in the context of *in vitro* cell culture and *in vivo* infection models. Our data suggest that *Rora* is expressed by activated CD4<sup>+</sup> T cells, and its expression correlates with effector function, such as the expression of Th lineage-defining transcription factors and the production of cytokines.

## Materials and methods

### Mice strains

**Rora reporter mice.** *Rora* T2A Teal reporter mice [14] were generated briefly as follows: A reporter cassette, encoding a short Gly-Ser-Gly linker peptide, FLAG epitope tag, T2A self-cleaving peptide and Teal fluorescent protein, followed by a loxP-flanked Neomycin cassette, was inserted (directly upstream of the) *Rora* stop codon. Successful targeting of JM8 ES cells was confirmed by Southern blot and the Neomycin cassette was removed from the resultant mice by inter-crossing with a Cre recombinase strain.

**Rora KO mice.** STOCK Tg(Cd4-cre)1Cwi/BfluJ mice were crossed with *Rora*<sup>tm1a</sup>(EUCOMM)<sup>Wtst</sup> mice. F1 progenies were crossed again, and F2 were tested for having at least one allele of Cd4-cre, and two alleles of *Rora-lox*.

### Overexpression of *Rora* and analysis

*Rora* was cloned into a retroviral vector (M6-mCherry-Cter) as follows. cDNA was made from RNA extracted from mouse spleens, following the protocol of SuperScript II reverse

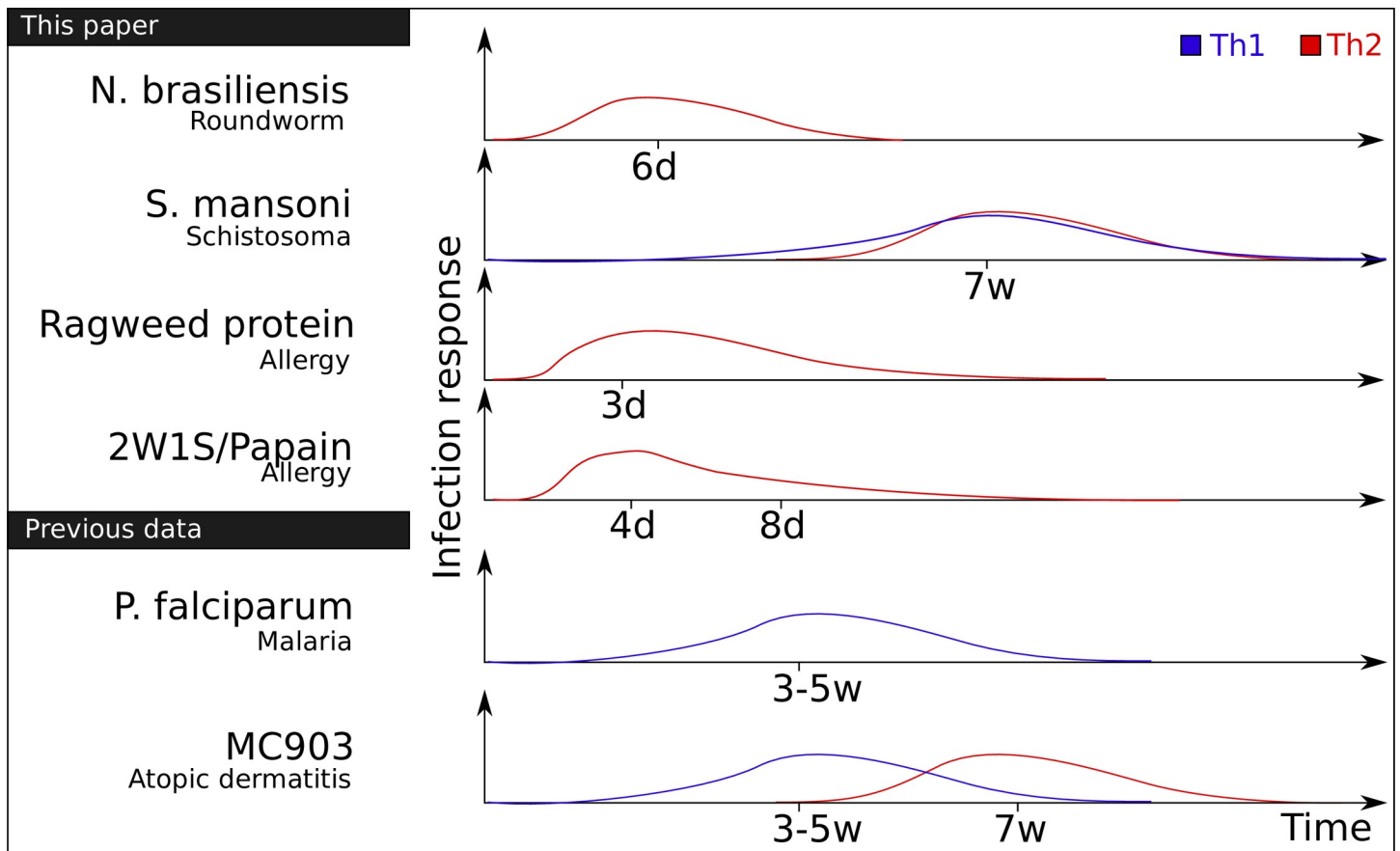


**Fig 1. Overview of the experiments.** The immune response to the infection models considered in this paper, over time, and which T helper cells are involved according to literature. The times denote approximate peak of cell counts according to previous studies, not the time points we have sampled.

<https://doi.org/10.1371/journal.pone.0251233.g001>

transcriptase (Thermo Fisher Scientific #18064014). Primers were designed against *Rora* isoform ENSMUST00000113624 (fwd: ATGTATTTTGTGATCGCAGCGATGAAAAGCTCAAATTGAA, rev: TTACCCATCGATTTGCATGGCTGGCTCAAATT). After PCR and gel purification, another round of PCR was done to add compatible overhangs (fwd: CGATaagccttATGTATTTTGTGATCGCAGC, rev: GaatgcgggccgcCCCATCGATTTGCATGG). The product and backbone were digested with HindIII-HF and NotI-HF (NEB), purified, and ligated using T4 ligase (NEB). Several clones were picked and sequence verified by sanger sequencing (M6-Rora2-mCherry). Two other constructs were also constructed analogously for ENSMUST0000034766 (M6-Rora1-mCherry and M6-Rora1-GFP).

The virus production, activation and transfection was done as previously, with the addition of IL4 [15]. The transfection was done into 3 biological replicates (JaxJ, 8 weeks old), each with the 3 constructs and the no-insert M6 as control. No puromycin was used for selection. Cells were harvested on day 4, FACS sorted, and libraries prepared using the Sanger institute standard pipeline. Sequencing was done on a HiSeq 2500.

The differentially expressed genes were called by DESeq2 [16] (normalized counts ~ treatment + mouse). Each of the constructs were analyzed. Of these, one had *Rora* as the most DE gene and was retained for further comparison (M6-Rora2-mCherry). Counts and condition matrices are provided in S2 File.

## Mice infection and cell isolation

***Nippostrongylus Brasiliensis* infection.** C57BL/6 female mice were subcutaneously injected with 100ul (300 live third stage *Nippostrongylus Brasiliensis* (*N. Brasiliensis*) larvae per dose), over two sites. MedLNs, mesLNs, spleens, lungs, or siLP were taken from infected mice, 3, 5, 7, 10 or 30 days after infection as well as from uninfected mice. At each time point, cells were isolated from medLNs and mesLNs, by smashing the tissue through 70μm cell strainers. Lungs were incubated in collagenase D (0.72mg/ml, Amersham, Bucks, UK) for 30min, smashed through 70μm cell strainers, and suspended in RBC lysis buffer (eBioscience Ltd). Spleens were smashed through 70μm cell strainers, and suspended in RBC lysis buffer. siLP cells were isolated from colonic tissue as previously described [17]. In brief, siLP cells were released by digestion of the tissue with RPMI/4-(2-hydroxyethyl)-1-piperazineethanesulfonic acid (HEPES) supplemented with 60 μg/ml DNaseI (Sigma), and 400 ng/ml of Liberase (Roche Applied Science, Burgess Hill, UK). Isolated cells were stained with conjugated antibodies for sorting (S3 File). For RT-qPCR and bulk RNA-seq experiments, single cells were sorted into the lysis buffer and were stored in -80°C.

Mice were weighed before the infection and daily during the experiment or until weights were deemed to be stable. Mice were monitored daily for clinical signs, including observations of the animal's extremities, abdomen, coat condition, behavior and weight. If clinical signs were observed, monitoring was carried out more frequently. Mice showing signs of ill health that were likely to exceed a moderate severity, were killed by a Schedule 1 method. Humane endpoints were determined utilising a tailored score sheet that incorporated observations of an animal's extremities, abdomen, coat condition, behavior and weight. No adverse events were experienced.

***Schistosoma mansoni* infection.** The complete life cycle of the parasite *S. mansoni* is maintained at the Wellcome Sanger Institute. Cercariae, the mammalian infective stage, were harvested by exposure of infected *Biomphalaria glabrata* snails to light for two hours in aquarium-conditioned water. Female C57BL/6 mice were infected with 300-mix sex *S. mansoni* cercariae via IP as described elsewhere [18]. Mice were checked twice a day for any sign of health deterioration. After 6 weeks post infection, mice were euthanized with an overdose of anaesthetic, adult worms were perfused from the mouse circulatory system as described previously [19], and mouse spleen and mesLNs were recovered surgically and placed in PBS for further processing. Cells were isolated from tissues and were stained for sorting. Activated T cells, CD3+CD4+CD44+SELL-, were sorted into a C1 chip and processed for RNA-seq.

The work using animals was carried out in accordance with the UK Animals (Scientific Procedures) Act under appropriate licenses issued by the Animals in Science Regulation Unit (ASRU) at the Home Office.

**Lung immune challenge models.** Mice were anaesthetised by isofluorane inhalation followed by intranasal administration of Ragweed pollen (100 μg per dose; Greer Laboratories, Lenoir, NC), papain (10 μg per dose; Sigma) or 2W1S peptide (10 μg per dose; Designer Bioscience), dissolved in 40 μl PBS at the indicated time points. The PE-conjugated I-A(b) 2W1S tetramer was obtained from the NIH Tetramer core.

On the first day of dosing, more than one health check was conducted in order to monitor any reactions the animal may have had to the substance administered. When it was clear there were no reactions, the mice were health-monitored once daily. The health and welfare of animals were monitored with reference to the limiting clinical sign parameters listed in the "LMB Animal Usage Guidelines". In addition to this, the severity status of the procedure was determined by observations of the animal's extremities, abdomen, coat condition, behavior and weight. Animals were observed after immunisation and any animals displaying signs of ill-

health were killed by a Schedule 1 method. Humane endpoints were determined utilising a tailored score sheet that incorporated observations of an animal's extremities, abdomen, coat condition, behavior and weight. No adverse events were experienced.

**Cell sorting.** Cells were sorted with a BD Influx Cell Sorter or SY3200 Synergy cell sorter (iCyt) and analysed on Fortessa or LSRII BD cell analyzers using FlowJo. Surface and intracellular stainings were carried out according to the eBioscience protocols. A full list of the antibodies used is provided in [S3 File](#).

**Histology.** Lung lobes were fixed for 48 hours in 10% neutral-buffered formalin (Sigma), washed in PBS and transported to AML Laboratories (Florida) for embedding, sectioning and staining with haematoxylin and eosin.

**Microscopy and image analysis.** Images were captured using a VHX keyence microscope, using objective #2D1510064 at magnification "200" (2.1495um/px). The 2D stitching feature was used to capture the entirety of each lung section. Two sections were imaged from each mouse, with focus automatically calibrated for each section. All images were acquired in one seating, with the same settings for brightness.

Image analysis was done in R using the EBImage package [20]. In brief, pixels corresponding to background, cytoplasm and nuclei were manually annotated in one image. A classifier was set up to separate pixels into the 3 classes based on manual inspection of the RGB space.

To estimate emphysema, the distribution of inner holes was calculated by first detecting non-background area. A binary dilation operation was applied to filter out 1–2 pixel holes caused by improper tissue detection. Segmentation was then performed to find disjunct regions. The area of each region was calculated.

From the histogram  $H$  of hole sizes, we estimate the unevenness (indicating emphysema, compensating for overall compression of slides due to fixation) as  $S = H_{99\%}/H_{80\%}$ . Other ranges were tested and gave a similar outcome. Veins, surrounding space, and other artifacts are filtered out above the 1% top percentile, while the lower percentile reflects tissue shrinkage. Alternatively, the score can be interpreted as a measure of hole size unevenness/variance. To test for emphysema in the *Rora* KO we fit a linear model  $S \sim \text{replicate} + \text{genotype}$ , with genotype = 1 for Cre and +/Flox, 2 for Cre and Flox/Flox, and 0 otherwise ( $p = 0.018$ ). A simpler t-test of +/+ vs Flox/Flox, not using any of the +/Flox samples, and ignoring replicate batch effects, gives  $p = 0.17$ . This is not significant but in the direction of the more inclusive linear model.

**In vivo bulk RNA-seq.** RNA was extracted with SPRI beads, followed by Smart-seq2. Read counts were estimated with Kallisto [21]. DE genes were estimated by DESeq2 [16] after counts had been rounded to the nearest integer count. Simple control vs treatment linear models were used. Counts and condition matrices are provided in [S2 File](#).

## Quantitative single-cell gene expression analysis

**Single cell RT-qPCR measurement and analysis.** Single-cell gene expression analysis was performed using BioMark 96.96 Dynamic Array platform (Fluidigm, San Francisco, CA) and TaqMan Gene Expression Assays (Applied Biosystems, Carlsbad, CA). Single cells were sorted into 5 $\mu$ L of CellsDirect reaction mix and immediately stored in -80C. Control wells containing no cells were included. On thawing, a mix containing 2.5 $\mu$ L gene specific 0.2x TaqMan gene expression assays (Applied Biosystems), 1.2  $\mu$ L CellsDirect RT/Taq mix, and 0.3  $\mu$ L TE buffer were added to each well. RT-PCR pre-amplification cycling conditions were: 50°C, 15min; 95°C, 2min; 22x(95°C, 15s; 60°C, 4min). Samples were diluted 1:5 in TE buffer and 6% were mixed with TaqMan Universal PCR Master Mix (Applied Biosystems). The sample mix and TaqMan assays were loaded separately into the wells of 96.96 Gene expression Dynamic

Arrays (Fluidigm) in presence of appropriate loading reagents. The arrays were read in a Bio-mark analysis system (Fluidigm).  $\Delta$ Ct values were calculated in reference to the average of *Atp5a1*, *Hprt1* and *Ubc*.

The expression of each gene was fit by a bivariate normal distribution (R mixtools package [22]) and a cut-off set at the average position between the lower and upper gaussian midpoints. Genes above this were considered expressed if above this cut-off. qPCR levels and metadata are provided in [S1 File](#).

***S. mansoni* C1 single cell RNA-seq and analysis.** For *S. mansoni*, three small (5–10  $\mu$ m) C1 Single-Cell Auto Prep IFC chips (Fluidigm) were primed and 5000 cells were sorted directly into the chip. To allow estimation of technical variability, 1  $\mu$ l of a 1:4000 dilution of ERCC (External RNA Controls Consortium) spike-in mix (Ambion, Life Technologies) was added to the lysis reagent. Cell capture sites were visually inspected one by one using a microscope. The capture sites that did not contain single cells were noted and were removed from downstream analysis. Reverse transcription and cDNA preamplification were performed using the SMARTer Ultra Low RNA kit (Clontech) and the Advantage 2 PCR kit according to the manufacturer's instructions on the C1 device. cDNA was harvested and diluted to 0.1–0.3 ng/ $\mu$ l and libraries were prepared in 96-well plates using a Nextera XT DNA Sample Preparation kit (Illumina) according to the protocol supplied by Fluidigm. Libraries were pooled and sequenced on an Illumina HiSeq2500 using paired-end 75-bp reads.

Salmon was used to estimate gene expression counts [23]. Poor quality libraries were eliminated using Scater [24] based on exonic and mitochondrial read counts. For all queries, a gene was considered expressed if the Log10 (1+normalized count) was above 0.5. Gene overlap was tested using Fisher's method. Counts and condition matrices are provided in [S2 File](#).

***N. brasiliensis* C1 single cell RNA-seq.** T cells from *N. brasiliensis* infected mice were captured with C1 analogously to the *S. mansoni* mice. The cells were sorted for CD3+CD4+SELL-, from mesLN, medLN, lung and spleens. This data is available but was not used due to low quality.

***N. brasiliensis* Smart-seq2 single-cell RNA-seq and analysis.** For this analysis we included CD3+CD4+SELL- cells from the lungs at 30 days after infection, CD3+CD4+Rora<sup>teal</sup>+ and CD3+CD4+Rora<sup>teal</sup>- cells from *N. brasiliensis* infected Rora<sup>+teal</sup> reporter mice. Further we include cells from lungs, spleens, medLN and mesLN from infected and uninfected Rora<sup>+teal</sup> mice, 7 days after infection.

Single cell transcriptomes were generated by using the Smartseq-2 protocol [25]. Single cells were sorted into 96 well plate that contained 5 $\mu$ l of Triton-X lysis buffer, 1  $\mu$ l of 10  $\mu$ M olido-dT30-VN, 1  $\mu$ l dNTP mix (25 mM each) and ERCC controls at a final dilution of 1:64m and immediately stored in -80°C. cDNA was submitted for the amplification for 25 cycles on an Alpha Cyclor 4 thermal cycler. Amplified cDNA went through two subsequent rounds of cleaning by using Agencourt AMPure XP beads (Beckman Coulter UK Ltd, High Wycombe, UK) at a 1.0x ratio on a liquid handler Zephyr G3 NGS Workstation (PerkinElmer) and eluted in 20ul of RNase free water. Purified cDNA was subjected to quality control using 1  $\mu$ l of cDNA on an Agilent 2100 BioAnalyser (Agilent Technologies, Santa Clara, CA, USA) using the Agilent High Sensitivity DNA kit. Samples were normalised to a concentration of 0.3 ng/ $\mu$ l. Nextera libraries were prepared using Nextera XT DNA Sample Preparation kit (Illumina) according to the protocol supplied by Fluidigm. The library preparation has been done in combination with benchtop liquid handlers: Zephyr G3 NGS Workstation (PerkinElmer) and Mantis (Formulatrix). Purified pool of Nextera libraries was subjected to quality control using 1  $\mu$ l of cDNA on an Agilent 2100 BioAnalyser using the Agilent High Sensitivity DNA kit.

Salmon v0.8.2 [23] was used to map the reads to ensembl cDNA reference GRCm38 to quantify the gene expression. Counts were used for all the analyses. Low quality cells with

>15% mitochondrial genes or <1500 total genes were filtered out. Seurat [26] was used for single-cell analysis: Highly variable genes were calculated ( $x.low.cutoff = 0$ ,  $x.high.cutoff = 5$ ,  $y.cutoff = 0.1$ ), PCA performed on these ( $pcs.compute = 50$ ), and t-SNE on the first 25 PCA components. Finally clustering was done ( $reduction.type = "pca"$ ,  $dims.use = 1:25$ ,  $resolution = 0.5$ ). Common marker genes were plotted on top of the clusters and the cluster identities were assigned manually (*Gata3*, *Tbx21*, *Foxp3*, *Sell*, and *Rorc*). The TCR sequences for each single T cell were assembled using TraCeR [27] which allowed the reconstruction of the TCRs from scRNA-seq data and their expression abundance, in addition to identification of the size, diversity and lineage relation of clonal subpopulations. Cells for which more than two alpha or beta chains were identified were excluded from further analysis. iNKT cells were detected by their characteristic TCRA gene segments (TRAV11–TRAJ18). Only CD4+ T cells were kept in the final plot; other cells remain annotated in the ArrayExpress submission. Counts and condition matrices are provided in [S2 File](#).

### Screening for upstream regulators of *Rora*

**Cell culture.** Naive CD4+ T helper cells were extracted from spleens of JaxJ mice, 8 weeks old males (Stem Cell Technologies #19765, CD8-CD11b-CD11c-CD19-CD24-CD25-CD44-CD45R-CD49b-TCR $\gamma/\delta$ -TER119-), according to the manufacturer's protocol. Up to 4 spleens were pooled in each biological replicate. The cells were activated in 96-well round bottom plates that were coated with 3 $\mu$ l/ml anti-CD3e (BioLegend #100202) and 5 $\mu$ l/ml anti-CD28 (BioLegend #102102) for 4 hours at 32°C. 24 hours later cytokines were added (See [S2 File](#), condition table). 72 hours after activation the cells were pelleted, resuspended in RLT buffer (Qiagen #79216), and stored at -80°C.

For the repeated screen, culturing was done in the same manner. The cells were then stained with PI and anti-CD4 eFluor 660 (eBioscience 50-0041-82, clone GK1.5) for 30 minutes in IMDM media. The cells were then FACS sorted to retain live CD4+ T cells, on average 5000 cells per well.

During Th0 conditions, it is possible for the cells to become somewhat Th1 polarized; we have looked at markers in the data but can neither confirm nor disprove that this is the case for these experiments.

**RNA-sequencing.** For the first screen, RNA was extracted using Agencourt AMPure XP beads (Catalog #A63881) at 1.5:1 ratio into 10 $\mu$ l elution volume. RNA-seq was done following Smart-seq2 [25] but with the following changes: The input was increased to 7 $\mu$ l and Mix 1 consisted of 2 $\mu$ l 10 $\mu$ M dNTP and 2.5 $\mu$ l 10 $\mu$ M oligo-dT. Mix 2 consisted of 5 $\mu$ l SmartScribe buffer, 5 $\mu$ l 5M Betaine, 1.25 $\mu$ l SmartScribe, 1.25 $\mu$ l (100 $\mu$ M) DTT, 0.15 $\mu$ l 1M MgCl<sub>2</sub>, 0.38 $\mu$ l 100 $\mu$ M TSO, and 0.47 $\mu$ l SUPERase inhibitor. SPRI cleanup was done at ratio 0.8:1 following first-strand synthesis, eluted into 12 $\mu$ l NFW. Mix 3 consisted of 12.5 $\mu$ l KAPA HiFi 2x master mix and 0.5 $\mu$ l 10 $\mu$ M ISPCR. PCR was done with 10 cycles. In the second screen, RNA-seq was done similarly with the following modification: No SPRI-cleanup was done after first-strand synthesis. Instead a larger amount of mix 3 was added directly.

On average 0.2ng cDNA was then used for Nextera XT library preparation, done at 25% of volume recommended by manufacturers protocol. Sequencing was done with 2 lanes of Illumina 50bp PE HiSeq 2500.

**Upstream analysis.** Salmon was used to estimate gene expression counts. Poor quality libraries were eliminated using Scater based on exonic and mitochondrial read counts. Genes with average normalized counts below 0.3 were removed. The increase/decrease in *Rora* expression level was computed by DEseq2 [16] using a linear model:  $\text{normalized counts} \sim \text{treatment} + \text{mouseReplicate}$ , where treatment is a factorial variable. The correlation heatmap

between treatments was calculated as  $\text{cor}(\text{cor}(\text{FC}))$ . The first correlation is used as a dimensionality reduction while the second correlation is used to remove the technical bias toward positive correlation. Clustering was done using R `hclust`, standard parameters.

The CellTrace FACS data was analyzed with FACSAnadu [28] to obtain cells in each division stage. The cell counts were analyzed across replicates and compared to controls using R.

## Metabolite LC-MS

Metabolites were extracted using a modification of a previous method [29]. Briefly, roughly 200k cells were resuspended in chloroform/methanol (2:1). After mixing samples, water was added (300  $\mu\text{L}$ ) and centrifuged at 13,000  $\times g$  for 20 min. The organic layer (lower fraction) was collected and dried under a stream of nitrogen. The organic fraction was reconstituted in chloroform/methanol (1:1; 100  $\mu\text{L}$ ) and 10  $\mu\text{L}$  were mixed in 90  $\mu\text{L}$  IPA/acetonitrile/water (2:1:1). The samples were analysed by LC-MS using an LTQ Orbitrap Elite Mass Spectrometer (Thermo Scientific). Sample (5  $\mu\text{L}$ ) was injected onto a C18 packed-tip column (75 $\mu\text{m}$   $\times$  100mm, Thermo Scientific) at 55°C. The mobile phase A was acetonitrile/water 60:40, 10 mM ammonium formate whilst B was LC-MS-grade acetonitrile/isopropanol 10:90, 10 mmol/L ammonium formate. In negative ion mode, ammonium acetate was used to aid ionisation. In both positive and negative ion mode, the gradient used (S5 File) was run at a flow rate 0.5 mL/min. Data were acquired with a mass range of 100–2000  $m/z$ . Chromatograms were converted to mzML format and annotated using an in-house R script. The annotated metabolites were size factor normalized to enable comparison. PCA was performed on the *in vitro* and *in vivo* samples separately (S1 Fig in S1 File). Lungs and spleens from *in vivo* samples appear to cluster together, suggesting no need to correct for tissue differences. *In vitro* samples were compared with Limma [30], with all naive cells (negatively selected as CD8-CD11b-CD11c-CD19-CD24-CD25-CD44-CD45R-CD49b-TCR $\gamma/\delta$ -TER119-) compared to all day 6 samples Th0/1/2. For the *in vivo* samples, we used the simplest model of  $\sim 1 + \text{isko}$ . Bayesian error correction was performed.

## Results and discussion

### *Rora* is expressed in activated CD4+ T helper cells *in vivo*

We wanted to get an overview of *Rora* expression in CD4+ T helper cells during worm infection. As most of the mouse models used in this study are type 2 immunity, we focus more specifically in Th2 cells. Mice were infected with *Nippostrongylus brasiliensis* (*N. brasiliensis*), a tissue migrating parasitic roundworm of rodents. *N. brasiliensis* initiates infection at the skin, the site of invasion, and then migrates via the circulatory system to the lungs. Through exploitation of host lung clearance, worms are transported to the intestine, from where they are expelled. In total, this infection is resolved within 7–10 days (Fig 1).

To get an overview of the infection at the molecular level, we performed single cell quantitative reverse transcription PCR (scRT-qPCR, Fluidigm Biomark). We prepared cells from the lungs, small intestine lamina propria (siLP), mediastinal lymph nodes (medLN) and mesenteric lymph nodes (mesLN) of mice, 3, 5 and 7 days after *N. brasiliensis* infection (Fig 2A). Tissues were also collected from uninfected mice as controls. Both CD3+CD4+SELL+ (naive) and CD3+CD4+SELL- (activated) cells were sorted. We examined 440 individual CD3+CD4+ T cells for the expression of 96 genes including housekeeping genes, different immune cell markers, T helper markers, cytokines, cytokine receptors, chemokine receptors, known and candidate regulators for Th cell differentiation (Fig 2B; S2 File). Consistent with a predominantly type-2 immune response, 70% of the CD3+CD4+SELL- cells expressed *Gata3*, whilst 26% expressed *Foxp3* and only 2% contained *Tbx21* or *Rorc*. Interestingly, in this population,



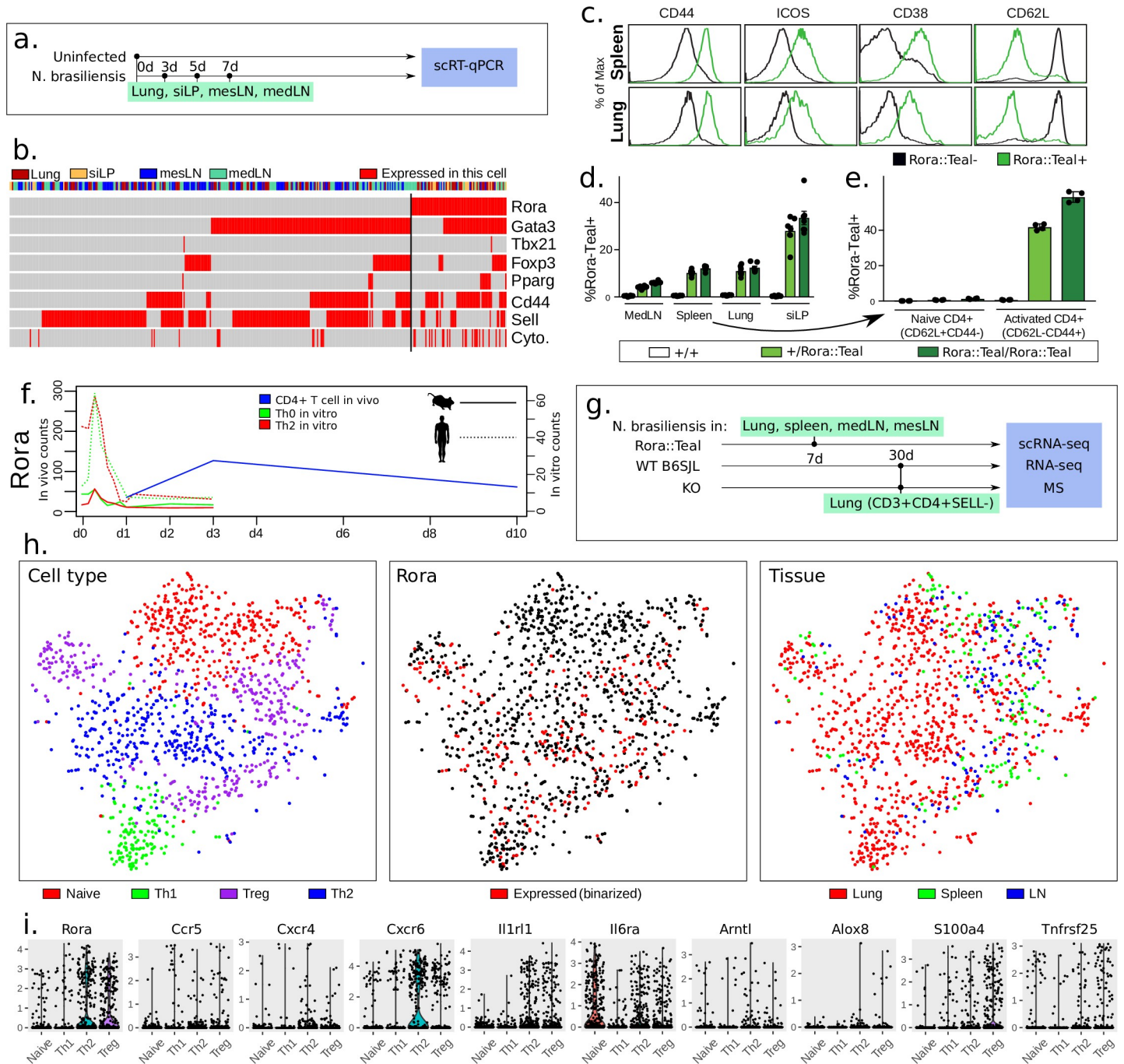


**Fig 2. Rora is expressed in activated T cells *in vivo*, with mainly spatial variation.** (a) Experimental design for single-cell RT-qPCR. (b) Gene expression according to RT-qPCR from CD4+ T cells during *N. brasiliensis* infection. *Gata3<sup>hi</sup>* cells, which we assume are Th2, are also expressing *Rora*. The category “Cytokines” refers to any of *Ifng*, *Il4*, *Il13*, *Il5*, *Il6*, *Il10* or *Il17a* being expressed. Top row denotes spatial location: Lung, gut (siLP), mesenteric and mediastinal lymph nodes (n = 4 mice). Every column is one individual cell. (c) Flow cytometric analysis of CD4+ T cells from the spleen and lung of Rora<sup>+/teal</sup> naive mice (black histogram = Rora<sup>teal-</sup> cells, green histogram = Rora<sup>teal+</sup> cells) (n = 23). All error bars are ±sample s.d. (d) Frequency of Rora<sup>teal</sup> expression across tissues, with siLP having the highest number (n = 12). (e) Fraction of naive (CD4+CD25-CD44-SELL+) or activated cells expressing Rora<sup>teal</sup>. RORA is mainly expressed in activated cells *in vivo* (n = 12). (f) *N. brasiliensis* Rora expression over time, overlaid with previously published mouse and human *in vitro* time course data of *Rora*, showing no or low expression of *Rora* in activated *in vitro* T cells. (g) Experimental design of scRNA-seq experiment, with (h) tSNE clustering of CD4+ T cells extracted from *N. brasiliensis* infected mice and measured by single-cell RNA-seq (1670 cells after filtering). We primarily identify Naive, Th1, Th2 and Treg cells, of which *Rora* is expressed in all non-naive cells. See methods and the provided code for the precise workflow. (i) Expression distribution of selected genes from the scRNA-seq data.

<https://doi.org/10.1371/journal.pone.0251233.g002>

we noted a significant overlap of *Gata3* and *Rora* (Fisher,  $p = 4 * 10^{-4}$ ), and also of *Rora* and *Foxp3* (Fisher,  $p = 2 * 10^{-4}$ ) (Fig 2B).

To investigate *Rora* activity in activated Th cells, we examined *Rora* expression using a *Rora*<sup>+/*teal*</sup> reporter mouse, in which the gene encoding Teal fluorescent protein has been inserted at the 3' end of the *Rora* coding sequence and expressed from a self-cleaving T2A site [14]. Flow cytometric analysis of reporter gene expression indicated that *Rora* was expressed in a proportion of CD4+ T cells isolated from medLN, spleen, lung and siLP (Fig 2C). We noted that all *Rora* expressing cells possessed an activated phenotype, as evidenced by their expression of CD44, ICOS and CD38 and down-regulation of SELL (Fig 2D). Accordingly, *Rora*<sup>+/*teal*</sup> T cells were therefore significantly enriched within the activated T cell subset, comprising 40–60% of this population, but absent from the pool of naive cells (CD4+CD25-CD44-SELL+) (Fig 2E). This correlation of *Rora* expression with T cell activation is in contrast with RNA-seq analysis made during the first 72h of *in vitro* culture of Th0 and Th2 cells, as previously reported (Fig 2F) [15]. There, in both mouse and human, *Rora* is expressed in naive cells, with a sudden increase around 2–4 hours of activation, before a gradual decrease in expression (overall slightly higher expression in Th2 over Th0). This agrees with another *in vitro* activation dataset where the *Rora* expression level is unchanged and low, in both Th17 and Th1 cells, following activation [31]. To compare with the *in vivo* situation, we generated RNA-seq data from CD4+ T cells, isolated from the spleens of *N. brasiliensis* infected wild-type mice 1, 3 and 10 days after infection, and overlapped with the *in vitro* data (Fig 2F). Here *Rora* is seen to increase, reaching a high and fairly sustained level around day 3. This is in agreement with a previous single-cell analysis of Th1/Tfh cells during malaria infection where *Rora* expression is seen to increase over time in Th1 [32] (S2A, S2B Fig in S1 File). It is also consistent with a study on atopic dermatitis [10], a study on Tregs [33] (S2C Fig in S1 File), as well as on T cells in a melanoma model [34] (S2D Fig in S1 File). Taken together, as *Rora* is consistently present *in vivo* but not *in vitro*, these 6 datasets suggest that *Rora* is induced not primarily by activation, but possibly by an external cue from the micro-environment.

Because the particular (micro-)environments might influence *Rora* expression, we examined our scRT-qPCR data across different organs (Fig 2B). Overall, the expression of *Rora* was relatively constant in CD3+CD4+ cells 3–7 days after infection (Fig 2F). However, in terms of tissue, it was expressed more frequently in the siLP and lungs, where 37% of cells expressed *Rora*, compared to 20% of the cells in lymph nodes. This pattern was confirmed using flow cytometry, where  $10.9 \pm 1.9\%$  of CD4+ cells in the lung were *Rora*<sup>+/*teal*</sup>,  $10.1 \pm 1.1\%$  from the spleen,  $27.9 \pm 5.8\%$  from the small intestine lamina propria and only  $4.0 \pm 0.6\%$  from medLN (Fig 2D). This tissue distribution likely reflects the relative frequency of activated Th cells in each location.

*Rora* has so far been seen in activated cells, partly overlapping with primary markers of Th2 and Treg (*Gata3* and *Foxp3*). To fully confirm the presence of *Rora* among different T helper cell types, as defined by the full transcriptional program, we used scRNA-seq on lymphoid and non-lymphoid tissue, isolating CD3+CD4+SELL- cells from the lungs 30 days after infection (*N. brasiliensis* infected wild-type mice 1, 3 and 10 days after infection, and overlapped with the *in vitro* data (Fig 2G). As reference points we included CD3+CD4+*Rora*<sup>teal+</sup> and CD3+CD4+*Rora*<sup>teal-</sup> cells from *N. brasiliensis* infected *Rora*<sup>+/*teal*</sup> reporter mice. Lungs, spleens, medLN and mesLN were also taken from infected and uninfected *Rora*<sup>+/*teal*</sup> mice, 7 days after infection. The cells were clustered and each cluster annotated using common markers (*Sell*, *Ifng*, *Gata3*, *Foxp3*) as Naive, Th1, Th2 and Treg cells (Fig 2H, all cells are shown in S2E Fig in S1 File). Cells from the lymph nodes and spleen are mainly Naive or Treg, otherwise the cell origin and T cell fate appear fairly uncorrelated. The distribution of *Rora* expression level

across the different CD4<sup>+</sup> T cell types was investigated (Fig 2H and 2I). Again, we note that *Rora* is expressed among all activated T cells (however, less induced in Th1).

To confirm that this distribution of *Rora* expression is not specific to the response to *N. brasiliensis* infection we compared it to another worm model, *Schistosoma mansoni* (*S. mansoni*). CD3<sup>+</sup>CD4<sup>+</sup>SELL<sup>-</sup> cells were collected 6 weeks after infection from spleens and mesLN (S2F Fig in S1 File). Single cell RNA-seq was performed and analysis shows that *Rora* is expressed in 59% of the activated cells (expressed defined as greater than zero counts). Approximately all (98%) cells that expressed *Rora* also expressed any of the key regulators *Gata3*, *Foxp3* or *Tbx21*.

To conclude, we have performed FACS, scRT-qPCR and scRNA-seq, and confirmed that *Rora* is generally expressed in a proportion of activated T cells during *N. brasiliensis* infection. *Rora* induction is likely to depend on a local environmental cue not present in the usual CD3/CD28 *in vitro* activation system. Thus an *in vivo* system is required to study the physiological role of *Rora*.

### **Rora is expressed in activated T helper cells during immune responses**

To further corroborate these findings, we also investigated a non-worm immunity model, Ragweed pollen (RWP), a common allergen which causes lung inflammation [35]. The *Rora*<sup>+teal</sup> reporter mice were exposed to intranasal RWP or PBS (Phosphate Buffered Saline, a negative control administration), administered every 2–3 days for 2 or 6 weeks (Fig 3A). As anticipated, RWP exposure resulted in increased CD4<sup>+</sup> T cell counts in the lung and mediastinal lymph node (medLN) after 2 weeks as compared to PBS controls, and this was maintained after 6 weeks of continuous RWP administration (Fig 3A). In lung, but not medLN, this increase in CD4<sup>+</sup> T cell frequency was accompanied by an elevated proportion of T cells expressing *Rora*, increasing from 30% to 40% between 2 and 6 weeks of RWP administration (Fig 3B and S3 Fig in S1 File). Consistent with our findings in untreated mice, *Rora*<sup>+teal</sup> T cells elicited by RWP stimulation had an activated phenotype, characterised by a CD44<sup>+</sup>SELL<sup>-</sup> surface profile (S3 Fig in S1 File). Notably, the *Rora*<sup>+teal</sup> T cell subset was enriched for cells that had acquired effector function, identified by their expression of the cytokines IFN $\gamma$ , IL-13 and IL-17A, or the Treg-associated transcription factor, FoxP3 (Fig 3C). Here again we note that *Rora* expressing cells include diverse activated cell phenotypes, that is, Th1, Th2 and Th17.

To understand the involvement of *Rora* in effector cells, we examined its expression in cytokine-expressing cells. From the *N. brasiliensis* model single-cell RT-qPCR, 83% of the cells that expressed either IL-4, IL-13 or IL-10, also expressed *Rora* (Fig 2B). The corresponding number in the *S. mansoni*-infected mice is 71% (S2F Fig in S1 File, scRNA-seq).

To investigate whether *Rora* was expressed by Th cells responding to secondary immune challenge, we challenged *Rora*<sup>+teal</sup> and control mice with 2W1S peptide intranasally, in conjunction with the protease allergen papain, which promotes a type-2 immune response (Fig 3D). After secondary immunisation with 2W1S/papain 3 weeks after the initial stimulation, we were able to identify 2W1S-responsive CD4<sup>+</sup> T cells by tetramer staining [36] and FACS analysis. Tetramer<sup>+</sup> CD4<sup>+</sup> T cells in both the lung and medLN were largely CD44<sup>+</sup> and *Rora*<sup>teal</sup> (Fig 3E), indicating that recently activated Th cells express *Rora*. As with the *N. brasiliensis* infection, in the *S. mansoni* model we found significant overlap of *Foxp3* and *Rora* in activated T cells (S2F Fig in S1 File, Fisher test,  $p = 2 * 10^{-4}$ ). A higher fraction of FOXP3<sup>+</sup> cells was also found in sorted *Rora*<sup>+teal</sup> relative to RORA<sup>-</sup> cells, in the RWP model (Fig 3C). The gap is increased when the exposure to the pollen was longer. The same could also be seen after mice were exposed to 2W1S+papain. The *Rora*<sup>+teal</sup> population contained 20% of the FOXP3<sup>+</sup> cells, while the RORA<sup>-</sup>, only 4% of the cells.

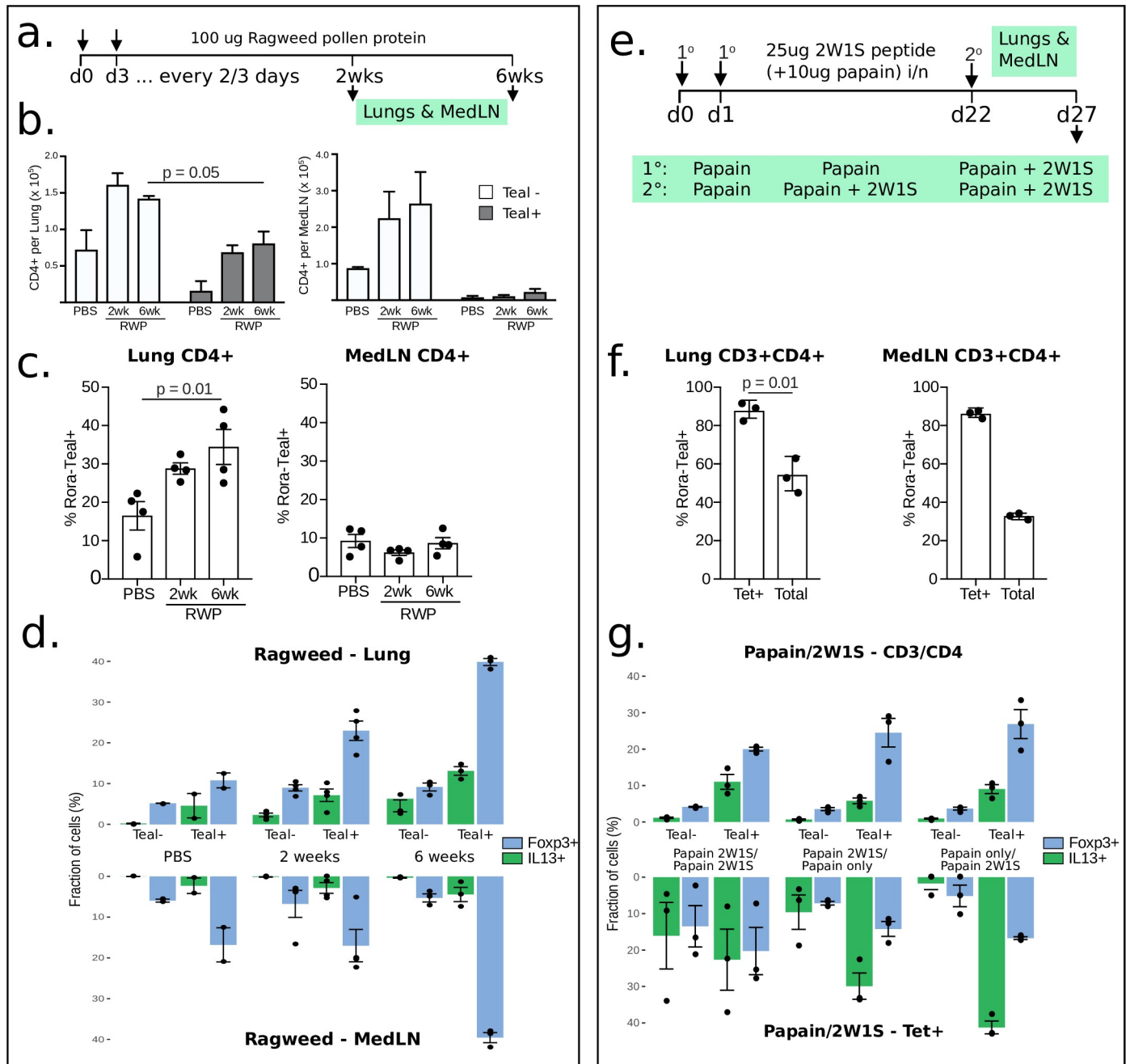


**Fig 3. *Rora* is generally expressed in Th2 during type 2 immunity.** All error bars are  $\pm$ sample s.d. (a) Design of ragweed flow cytometry experiment. (b) Flow cytometry analysis of CD4+ T cells from mice challenged with Ragweed pollen protein for 2 or 6 weeks, showing that *Rora* is expressed in lungs also during allergy. The Tetramer+ cells fraction among all T cells ranged between 0.5–2%. Here the number of *Rora*<sup>teal+/-</sup> cells are shown over time (n = 12, one repeat). (c) RORA expression in CD4+ cells increases in the lungs but not in MedLN during the ragweed challenge (n = 12, one repeat). (d) Flow cytometry analysis diagrams showing higher proportions of cytokines-expression and Tregs cells in *Rora*<sup>teal+</sup> sorted cells vs the *Rora*<sup>teal-</sup>, after Ragweed pollen protein exposure (n = 2). IL17 and IFN $\gamma$  were also measured (S2B Fig in S1 File) (note that we only did this experiment once). (e) 2W1S/papain challenge experimental design. (f) Flow cytometry analysis when T cells are challenged twice with 2W1S/papain, again confirming the presence of *Rora* in tetramer+ cells. Note that we only performed this experiment once (n = 3+3). (g) Flow cytometry analysis diagrams showing higher proportions of cytokines-expression and Tregs cells in *Rora*<sup>teal+</sup> sorted cells vs the *Rora*<sup>teal-</sup>, after 2W1S/Papain challenge (note that we only did this experiment once).

<https://doi.org/10.1371/journal.pone.0251233.g003>

Overall our data show that *Rora* is expressed in Th cells in worm immune models as well as in allergen type 2 immunity. We find *Rora* transcripts present in activated Th cells, not only in Tregs, but also in Th1 and Th2, as well as activated CD4+ T cells responding to a secondary immune challenge. *Rora* is also more correlated with cytokine-releasing cells, which suggests a function in effector cells.

### **Rora KO affects inflammation severity**

To isolate the *in vivo* physiological function of *Rora* in Th cells, we created a conditional knockout mouse line, where exon 4 of the *Rora* gene was deleted only in CD4+ cells ( $CD4^{cre}Rora^{fl/fl}$ ), verified by RNA-seq, S3A Fig in [S1 File](#)), resulting in a dysfunctional RORA protein. We noted no change in Th cell number when comparing  $CD4^{cre}Rora^{fl/fl}$  to control (S3B Fig in [S1 File](#)). We then infected  $CD4^{cre}Rora^{fl/fl}$  mice with *N. brasiliensis* and examined lung inflammation after 30 days. An unbiased image analysis algorithm was developed to detect emphysema and score stained lung sections ([Fig 4A](#)). Generally, uninfected samples score the lowest for emphysema, as expected ([Fig 4B and 4C](#)). During infection, single-allele *Rora* KO ( $CD4^{cre}Rora^{+/fl}$ ) had a higher score of emphysema, and double-allele KO ( $CD4^{cre}Rora^{fl/fl}$ ) even higher score (linear model fit,  $p = 0.018$ ). We detected no differences in our negative controls, no-Cre KO mice ( $Rora^{fl/fl}$ ), and WT with Cre KO mice ( $CD4^{cre}$ ). As emphysema can be caused by eosinophil infiltration, in analogy with a previous model [13] we analyzed eosinophil infiltration rate and noted an increase but not statistically significant difference (S3C Fig in [S1 File](#)).

We conclude that *Rora* expression in CD4+ T cells modestly promotes lung inflammation associated with *N. brasiliensis* infection. This may reflect a role for *Rora* in regulating the activity of T helper cells, and may also result from the modulation of Treg activity, as has previously been reported for *Rora*+ Tregs in skin [13].

### **Rora overexpression affects several key immune regulatory genes**

To probe the role of *Rora* in T cells, we next proceeded to identify the molecular targets of *Rora* in Th2 cells by means of retroviral overexpression. Th2 cells were induced *in vitro*, infected the day after induction, and on day 5, gene expression was compared by RNA-seq (empty viral vector vs overexpression vector, [Fig 5A and 5B](#)). The *in vitro* differentially expressed (DE) genes were compared to the genes that are differentially expressed between skin Tregs from wt vs  $CD4^{cre}Rora^{fl/fl}$  mice ([Fig 5C](#)). Consistent with a previous report [13], we see a strong effect on *tumor necrosis factor receptor superfamily member 25* (*Tnfrsf25*), which has been shown to be required for Th2 effector function, e.g., allergic lung inflammation [37]. The receptors *C-C chemokine receptor type 2* (*Ccr2*), *Ccr5*, and *Tnfrsf23* are in agreement, although with lower fold changes. We also find *Ninjurin 2* (*Ninj2*) which has recently been implicated in endothelial inflammation [38].

We also looked at a previous dataset of *Rora* small interfering RNA (siRNA)-treated human Th17 cells [39] and find that *Tnfrsf25* is DE ( $p = 2.2 \times 10^{-4}$ , DESeq2). In another study of Tregs during steady-state in mouse [40], we find that *Tnfrsf25* is higher in colon Tregs than in lymphoid tissue Tregs ( $p = 2 \times 10^{-2}$ , DESeq2). Thus four datasets, in different T helper cell types, confirm *Tnfrsf25* as a downstream gene.

Overall the two *in vitro* systems strengthen the claim of *Rora* as regulator of *Tnfrsf25*. However the expression of *Tnfrsf25* across Th2, Treg and Naive, but not Th1 ([Fig 2I](#)), shows that the function of *Rora* is not limited to Treg cells.

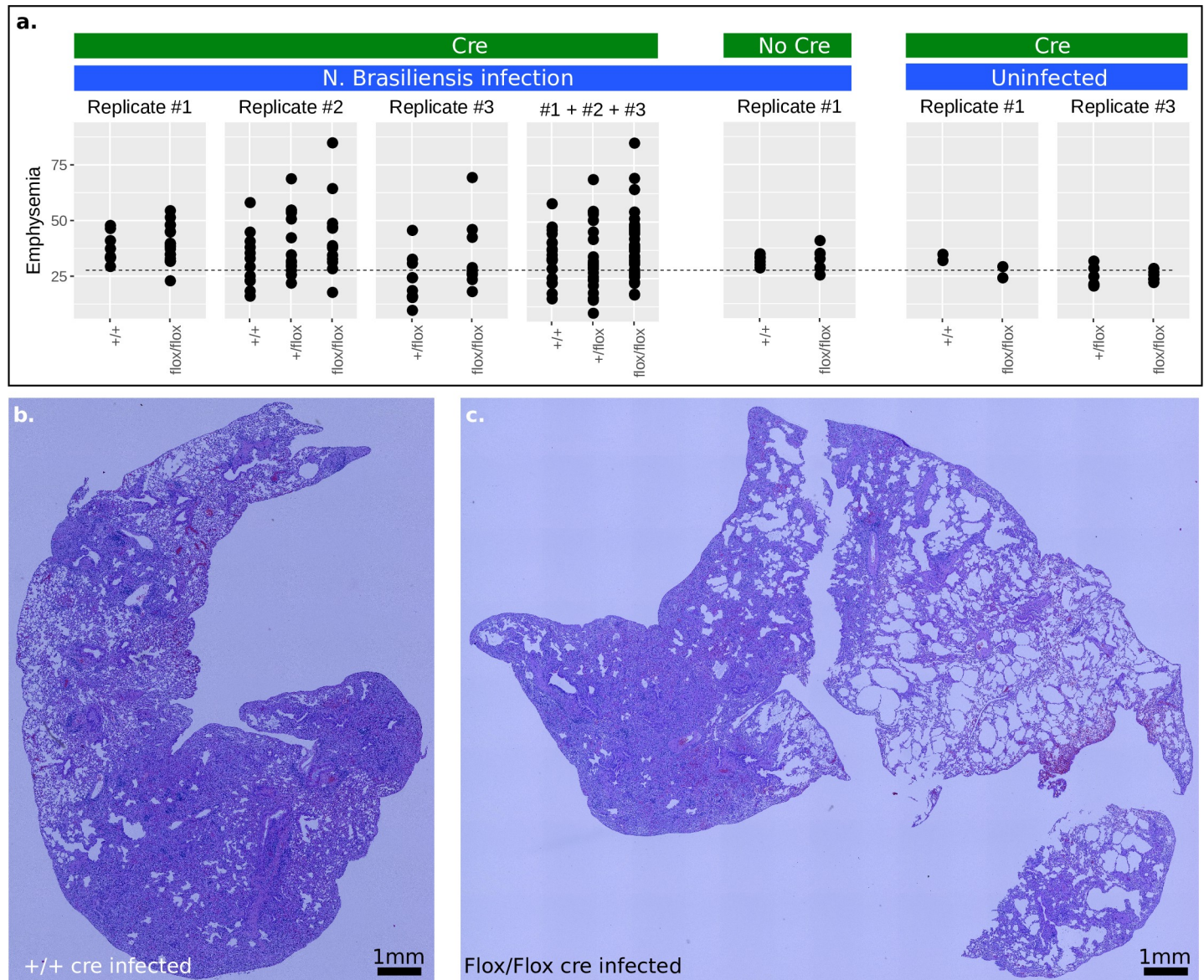


**Fig 4. *Rora* KO affects lung inflammation severity.** (a) Assessment of lung emphysema after *N. brasiliensis* infection, day 30 past infection, by microscopy and automated image analysis. Controls are included for no-Cre (against the *Rora*-Flox) and no infection (from left to right,  $n = 8, 17, 1, 14, 12, 9, 10, 29, 20, 39, 6, 6, 2, 2, 6, 6$ ). (b-c) Lung lobes were fixed, embedded, sectioned and stained with haematoxylin and eosin. The pictures represent the least and most inflamed lung sections as detected by the algorithm, located in +/+ and Flox/Flox (control and KO).

<https://doi.org/10.1371/journal.pone.0251233.g004>

### *Rora* affects activation *in vivo*

To see if *Rora* has additional functions *in vivo*, we generated bulk RNA-seq from activated (SELL-/CD44+) CD4+ T cells from control and  $CD4^{cre}Rora^{fl/fl}$  mice from lung, spleen, siLP and colon (30 days after *N. brasiliensis* infection), and compared the DE genes between the different tissues, the overexpression DE genes, and the previous Treg *Rora* KO data. Volcano plots are shown in Fig 5E (full list of fold changes in S2 File). From manual comparisons of these conditions, we have tried to find DE genes in common between the tissues, and if these in turn can explain the function of *Rora*. We generally do not see any DE cytokines of high statistical significance, but highlight some other types of genes here.

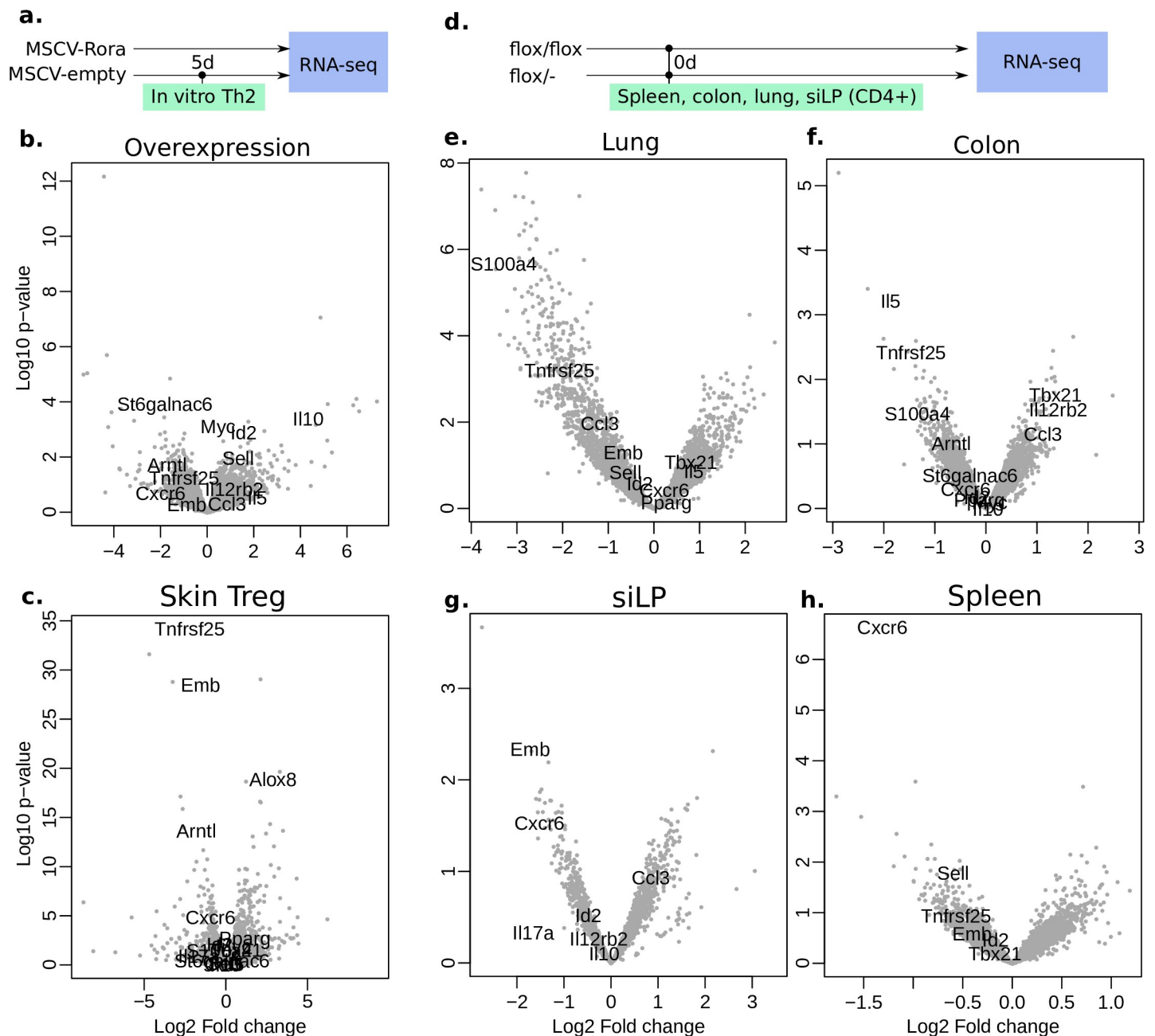


**Fig 5. Differentially expressed downstream genes of *Rora*.** To increase readability, only some gene names are written out (full DE gene data is in [S2 File](#)). (a) Design of the *in vitro* overexpression experiment. (b) *Rora* overexpression. (c) Previous data, DE genes in Treg from skin [13] (d) Design of the *in vivo* KO experiment. (e-h) DE genes *in vivo*, activated CD4+ T cells (n = 3+3), from lung, colon, siLP and spleen.

<https://doi.org/10.1371/journal.pone.0251233.g005>

We find the transcription factor *Aryl hydrocarbon receptor nuclear translocator-like (Arntl)* to be differentially expressed in activated CD4+ T cells from siLP as well as in the overexpression analysis and in Tregs in skin (Fig 5B and 5C). *Arntl* is involved in the circadian responsiveness, and is expressed in CD4+ T cells [41]. The *Arntl* promoter contains ROR elements (RORE), and was found to be regulated by *Rora* in mice [42]. RORA promotes *Arntl* expression and thereby maintains the circadian rhythm. We find it to be expressed in all cell types (Fig 2I).

The *S100 calcium-binding protein A4 (S100a4)* is another gene which is differentially expressed in activated T cells from lung, colon, and to lesser extent in Tregs in skin. In the single cell dataset, it is expressed mostly in Tregs but generally in Th1/Th2 (Fig 2H). It exists in both intra- and extracellular forms and can activate NF- $\kappa$ B [43]. Using an antibody, *S100a4* has been shown to mediate T cell accumulation, and Th1/Th2 polarization, at tumour sites [44]. Thus *S100a4* might act downstream of *Rora* to control T cell activation.

C-X-C chemokine receptor type 6 (*Cxcr6*) is differentially expressed in siLP, spleen and in Tregs in skin, and is consistently regulated in other tissues. *Cxcr6* is expressed in all Th cells but mostly in Th2 cells (Fig 2I). It might be involved in Th cell activation [45, 46].

The sialyltransferase *St6galnac3* is downregulated in colon and overexpression (Fig 5B and 5F). This enzyme transfers sialic acids to glycolipids and glycoproteins. Along with the previously DE gene *Alox8* (Fig 2I), we wondered if *Rora* may have any function on lipid metabolism. RORA has already been found to bind cholesterol [47] and is evolutionarily related to the nuclear receptor and lipid metabolism gene *Peroxisome proliferator-activated receptor gamma (Pparg)* [48]. We performed lipid LC-MS on *in vivo* *CD4<sup>cre</sup>Rora<sup>fl/fl</sup>* and WT cells from *N. brasiliensis* infected mice, as well as on *in vitro* WT naive and mature Th0/Th1/Th2 cells for reference (S4 Fig in S1 File, cells from negative magnetic bead selection as described in methods). The *CD4<sup>cre</sup>Rora<sup>fl/fl</sup>* presented small differences, and little overlap with the 85 lipids changed *in vitro* the first 6 days (cutoff  $p = 0.05$ ). However, all the top DE lipids are phosphocholines or phosphoethanolamines, and some phosphocholines can induce a type 2 immune response [49]. All the differentially expressed lipids are listed in S5 File.

In the spleen, *Sell* is downregulated in the KO (however it is still expressed as other cells are included as well), and opposite in the previous overexpression. This fits the idea of *Rora* driving activation and exit from the spleen, but why is it not DE in the other organs? We speculate that once a T cell has left the spleen or a lymph node, *Rora* might have already filled its purpose, and thus the effect on *Sell* will be smaller in any peripheral tissue.

We further noted the gene *Emb* (Embigin) in which is significantly DE in siLP, and in the same direction in overexpression, lung and spleen. It was also strongly DE in the previous skin Treg dataset. It has been shown to regulate cell motility in pancreatic cancer, and be controlled through the TGF- $\beta$  pathway [50]. It is possible that it could have a similar role in T cells.

Overall we see that *Rora* affects several genes *in vivo*, that are differentially expressed between different T helper cell types. Several of the downstream genes may explain the effect of *Rora*, including for example *Arntl*, *Cxcr6*, *St6galnac3*, *Emb* and *Sell*. However, *Rora* abrogation does not abolish T cells. It is possible that *Rora* acts as a helper factor, or tissue residence checkpoint, for T cell activation and migration.

## **Rora expression can be extrinsically regulated**

A remaining question is which genes regulate *Rora*, and whether regulation is solely due to the T cell itself or from an external signal. More insights into when *Rora* is induced would provide understanding of its role. As previously seen, *Rora* is generally not expressed during *in vitro* activation, but is upregulated during *in vivo* activation. This discrepancy may be explained by an unknown signal from the environment that is present *in vivo* but not *in vitro*. To find candidate upregulators we screened for *in vitro* upregulated genes during 39 treatments, including cytokines and chemokines, with 15 unstimulated controls, in 3 biological replicates. In short, naive cells were taken from wild type mouse spleens, plated on CD3/CD28 coated plates, with addition of test cytokines/chemokines 24 hours later. 5 days after plating the cells were measured by bulk RNA-seq (Fig 6A).

The stimulants and their effects are shown in Fig 6B (DE genes in S2 File). To validate our perturbation assay we looked at known marker genes. Of the genes having the strongest effect



we find the expected genes: IL4 for *Gata3* (Th2), Transforming growth factor beta 1 (TGFb1) for *Foxp3* (Treg), IL6 and partially TGFb1 and IL21 for *Rorc* (Th17) [51] (S5a-S5c Fig in [S1 File](#)). We then looked for the effect on *Rora* expression. The most upregulating stimulants are CCL5, IL15 and IL33.

CCL5 is chemotactic for T cells, eosinophils, and basophils. CCL5 signaling through CCR3 has been reported to regulate Th2 (IL4+CD4+) cellular responses to promote metastasis of luminal breast cancers [52]. Interestingly also CCR5, another CCL5 receptor, was upregulated during overexpression, implicating a potential autocrine role for this factor. *In vitro*, CCR3 and CCR5 are expressed primarily in Th1, Th2 and Th17 [31].

IL15 is produced by non-lymphoid cells and important for the survival of several lymphoid subsets [53]. IL15 KO mice are markedly lymphopenic due to decreased proliferation and decreasing homing to peripheral lymph nodes [54]. Increase in IL15 thus fits our observation of *Rora* expression primarily in activated Th cells outside the lymph nodes. *Il15ra* is expressed in all murine CD4+ T cell subsets [31].

IL6 resulted in upregulation of *Rora* (statistical test significant if both batches of IL6 are pooled), consistent with previous IL6 *in vitro* culture data [31]. IL6 has several roles, beyond generating Th17 cells *in vitro*, both pro- and anti-inflammatory [55]. *Il6ra* is expressed in all CD4+ T cell subsets [31], though in our scRNA-seq data less in Th1 (Fig 2I).

IL33 also induces *Rora*, and is mainly associated with Th2 or ILC2 cells [56]. This agrees with our *in vivo* scRNA-seq where *Rora* is slightly elevated in Th2 cells compared to other Th subtypes (Fig 2I). Our scRNA-seq shows that the corresponding receptor *Il1rl1* is expressed in all CD4+ T cell subsets but primarily in Th2 and Treg (Fig 2I).

*Ccl7* upregulates *Rora* and can do so through several receptors; these include for example CCR1, CCR2, CCR3, CCR5, and CCR10 [57]. All of these receptors are present in CD4+ T cells to some extent, but *Ccr5* is somewhat higher expressed than the rest [31].

The most downregulating stimulants are C-C motif chemokine 22 (CCL22) and stromal cell-derived factor 1 (SDF1a). CCL22 is secreted by dendritic cells and macrophages, and is suggested to induce Treg cell infiltration into the pleural space in patients with malignant effusion [58, 59]. In addition, its receptor CCR4 is required for CD4+ T cell migration to the skin [60]. In bulk *in vitro* data it is present in all CD4+ T cell subsets, especially after activation [31].

SDF1a (also known as CXCL12), a ligand for the chemokine receptor CXCR4, promotes bone marrow homing for T cells. It has been shown that Naive T cells downregulate CXCR4 to avoid this [61]. A further look at the Human Protein Atlas shows the tissues with expression of SDF1a to be particularly high in spleen, cervix/endometrium, and adipose tissue. In our study we compared with lung and gut, which have less *Cxcl12* expressed. This is consistent with our screening data, suggesting SDF1a may be a negative regulator of *Rora*. *Cxcr4* is expressed in all CD4+ T cell subsets at roughly equal level [31] according to bulk and our scRNA-seq data (Fig 2I).

To further validate if a treatment induces *Rora*, we also checked if a treatment induces the same downstream genes as in the *Rora* overexpression experiment. To do this we took genes from the *Rora* overexpression with a Log2 fold change > 2, and correlated the fold change with the corresponding fold change in a treatment (Fig 6C). Many of the most *Rora* influencing treatments also score similarly by this score. In particular, IL33 and CCL7 have a high level of agreement, followed by CCL22 (replicate a). Other treatments appear to have a less direct effect on *Rora*, for example IL6.

Based on our and previous data we conclude that *Rora* expression is mainly associated with an inflammatory state. Several cytokines may influence the expression of *Rora*. The effect on other genes can be studied using a similar screening approach, based on our supplementary data.

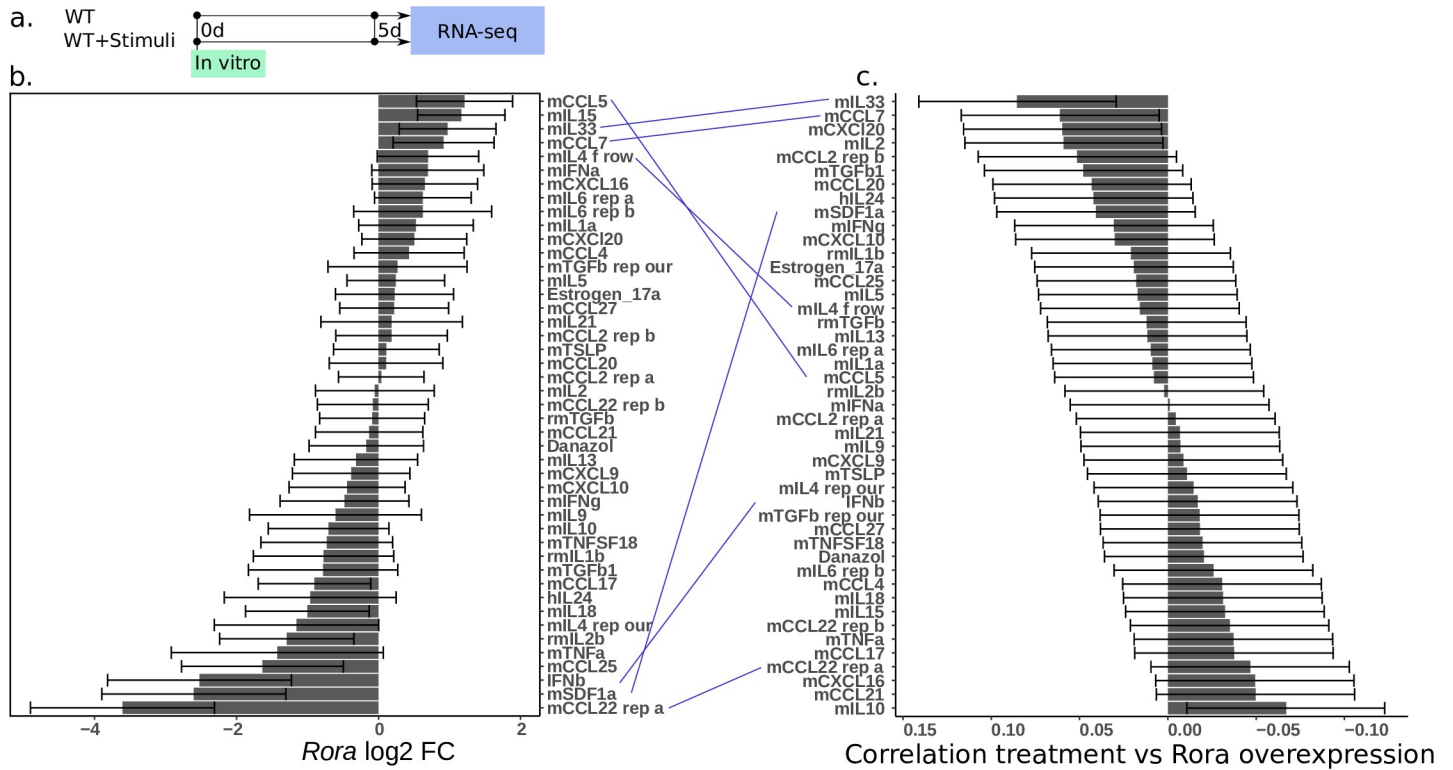


**Fig 6. A screen of cytokine-treated T helper cells reveals genes upstream of *Rora*.** The full list of stimuli, and the effect on any gene of interest, is provided in [S2 File](#). All error bars are  $\pm$ sample s.d. (a) Design of the *in vitro* experiment (b) Effect of all tested stimuli on *Rora* expression. (c) Global correlation of gene fold change in each stimulus, with fold change of gene expression during *Rora* overexpression. Lines have been drawn across panels b-c to highlight how similar a treatment is to directly perturbing *Rora*.

<https://doi.org/10.1371/journal.pone.0251233.g006>

### Conclusions

We have here investigated the impact of *Rora* on different subsets of CD4+ T cells, with an emphasis on Th2 cells, in several *in vivo* immune models. *Rora* is already known to be important for Th17 identity [12], and more recently it was discovered to regulate the function of Tregs in the skin [13]. Here we show that *Rora* is actually expressed in all activated T helper cells during different types of inflammation, including worm infections and allergy. We expand on the previous literature and suggest that *Rora* plays a wider role in the regulation of the immune response, in many T helper cell types—Th1, Th2 and secondary activated cells as well. Its function is likely to also involve further key downstream genes than just the previously shown *Tnfrsf25*. Our model of the *Rora* regulatory network is depicted in [Fig 7](#).

*Rora* deletion did not alter the overall CD4+ T cell numbers, and therefore does not seem to be involved in T cell proliferation. This was also shown before in a study where Th2 cells were examined in ROR $\alpha$ -deficient Staggerer mice [62]. In this study we found that Th2 cells from the ROR $\alpha$ -deficient mice were still able to differentiate and proliferate. However, we noticed higher inflammation in the lungs of CD4<sup>cre</sup>*Rora*<sup>fl/fl</sup> mice, after *N. brasiliensis* infection, indicating a functional role in CD4+ T cells. A similar effect was shown in skin, when *Rora* was deleted in Tregs only [13]. The effect was demonstrated to be through Treg *Tnfrsf25* signaling. *Tnfrsf25* has been shown to be required also for Th2 cell function in lung inflammation [37]. Our analysis of the DE genes of activated Th cells, in the lung and colon of worm infected mice, as well as overexpression, and reanalysis of previously published data, confirms the

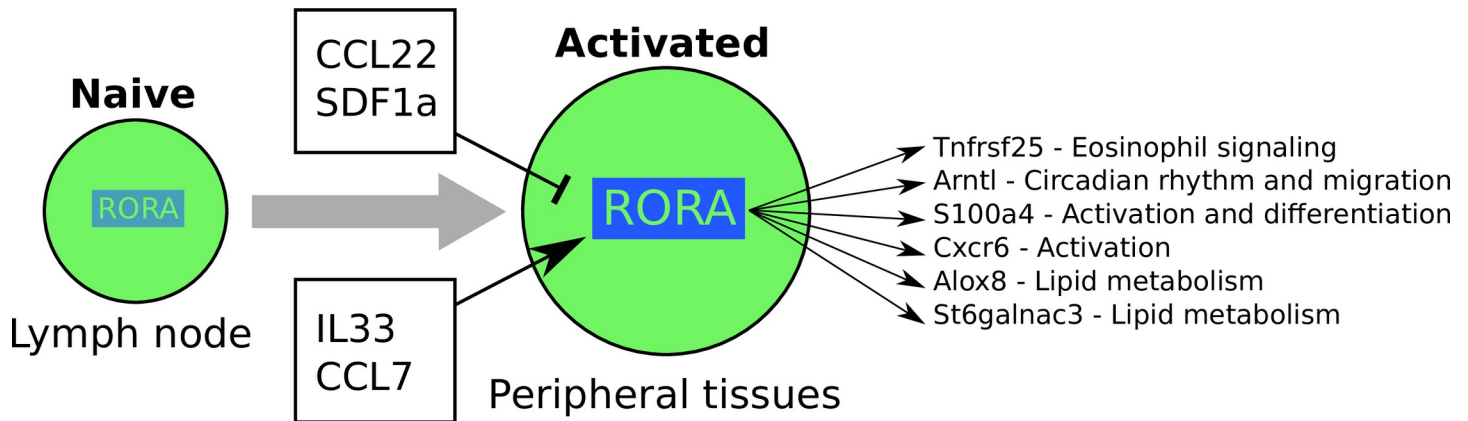


**Fig 7. Summary model.** *Rora* is expressed upon activation, and relies on additional stimuli from peripheral tissues for full induction of gene expression. Several cytokines have an impact on *Rora* expression level. *Rora* affects a diverse set of genes of importance for activated T cells, including *Tnfrsf25* (negative regulation of Eosinophils during infection), *Arntl* (circadian rhythm), *S100a4* (activation), *Alox8* and *Stgalnac3* (lipid metabolism).

<https://doi.org/10.1371/journal.pone.0251233.g007>

importance of *Tnfrsf25* in Tregs, but that its origin may include also other activated T helper cell subsets.

A higher fraction of activated T helper cells (both Th and Tregs) contained *Rora*, when located in non-lymphoid tissues (lung and siLP) compared to lymph node tissues. The same pattern was previously shown for skin-located *versus* LN-located Tregs [13]. The enrichment of *Rora*<sup>+/*teal*</sup> cells in peripheral tissues may reflect its correlation with T cell activation and effector function, or alternatively may relate to a role in influencing T cell migration. Our data is also unable to conclusively show if *Rora* is expressed before or after cytokines are expressed. Further research is required to see how *Rora* is involved in these regulatory programs.

One theory is that *Rora* has a complex interaction with circadian rhythm genes. T cells migrate in and out of the lymph node throughout the day [63], and *Rora* is already known to be involved in circadian rhythm. Our data strengthens this claim as the circadian gene *Arntl* is DE in both Tregs and other activated CD4<sup>+</sup> T cells, in agreement with previous studies [42, 64]. It is possible that *Rora* is regulated through external signalling. We investigated this with a small screen and found, for example, SDF1a as a negative regulator. This could be interpreted in the context of leukocyte migration during circadian rhythms, as blocking SDF1a disables the circadian migration of leukocytes [63]. A caveat with the circadian rhythm influence is that, if the *Rora* RNA cycles over the day, so will the Rora protein—but with a delay induced by translation speed. This significantly complicates the interpretation of our data, and possibly helps explain any discrepancies in our RNA-seq vs FACS analysis. Further detailed work is required to account for any circadian effects.

Other theories can be brought forward based on DE genes downstream of *Rora*. If *Sell* is a direct downstream gene, it would explain most of the activation. However, other downstream genes such as *S100a4*, *Emb* and *Cxcr6* have also been linked to activation and cell migration. As *Rora* is a transcription factor which may have thousands of direct targets, the effect may be through more than one downstream gene, making it hard to pinpoint a single molecular mechanism.

The previous *Rora* KO sg mice display a range of phenotypes, e.g., reduced body weight gain and neuronal disorders. Assuming the gene regulatory network is preserved in other cell types, our work provides hypothetical mechanisms to explore further in future experiments. Since *Rora* controls PPARα [65], it may be a possible intermediate, with our data suggesting effects on phosphocholines. In this work we did not investigate the effect of potential *Rora*

ligands but these could further contribute to a feedback loop. As for the neuronal disorders, knowing that the SDF1a-CXCR4 interaction is also important for neuronal guidance [66], SDF1a-mediated regulation of *Rora* may also explain neuronal impacts.

In conclusion, *Rora* has been found to be important for several immune cell types, in different contexts. It is involved in multiple pathways and appears to link cell migration with cell cycle, but also affects the outcome of inflammation through, but not limited to, *Tnfrsf25*. In its natural context, *Rora* is mainly associated with non-lymphoid tissue and activated T cells. *In vitro* culture suggests that this is due to environmental stimuli, possibly SDF1a. By generating a large systematic transcriptomic characterization of cytokine effects on T helper cells, we have found several cytokines that may explain be responsible for *Rora* induction in other tissues. With the large number of conditions tested in this study we are one step closer to understanding the multiple functions of this gene.

## Supporting information

**S1 File. Collection of supplementary S1–S5 Figs.**

(PDF)

**S2 File. RNA-seq count data and condition matrices.**

(ZIP)

**S3 File. List of antibodies.**

(CSV)

**S4 File. Biomark single cell RT-qPCR data, raw data and list of TaqMan probes.**

(ZIP)

**S5 File. LC-MS lipid data.**

(ZIP)

## Acknowledgments

We would like to thank Helen Jolin for help with mice, MRC Ares and Biomed staff, and Bee Ling Ng, Chris Hall, Jennie Graham, Maria Daly, Fan Zhang and Martyn Balmont for help with cell sorting. Ayesha Jinat provided technical assistance with RNA-seq.

## Author Contributions

**Conceptualization:** Liora Haim-Vilmovsky, Johan Henriksson, Jennifer A. Walker, John C. Marioni, Andrew N. J. McKenzie, Sarah A. Teichmann.

**Data curation:** Liora Haim-Vilmovsky, Johan Henriksson, Jennifer A. Walker, Eviatar Natan.

**Formal analysis:** Johan Henriksson, Zhichao Miao, Gozde Kar, Steven Woodhouse, Mirjana Efremova.

**Funding acquisition:** Liora Haim-Vilmovsky, Sarah A. Teichmann.

**Investigation:** Liora Haim-Vilmovsky, Johan Henriksson, Jennifer A. Walker, Eviatar Natan, Simon Clare, Jillian L. Barlow, Evelina Charidemou, Lira Mamanova, Xi Chen, Valentina Proserpio, Jhuma Pramanik, Anna V. Protasio.

**Methodology:** Liora Haim-Vilmovsky, Johan Henriksson, Jennifer A. Walker.

**Project administration:** Liora Haim-Vilmovsky, Johan Henriksson.

**Resources:** Liora Haim-Vilmovsky, Johan Henriksson, Julian L. Griffin, Matt Berriman, Gordon Dougan, Jasmin Fisher, John C. Marioni, Andrew N. J. McKenzie.

**Software:** Johan Henriksson.

**Supervision:** Liora Haim-Vilmovsky, Jasmin Fisher, John C. Marioni, Andrew N. J. McKenzie, Sarah A. Teichmann.

**Validation:** Liora Haim-Vilmovsky, Johan Henriksson, Jennifer A. Walker, Eviatar Natan, Jillian L. Barlow.

**Visualization:** Liora Haim-Vilmovsky, Johan Henriksson.

**Writing – original draft:** Liora Haim-Vilmovsky, Johan Henriksson, Jennifer A. Walker, John C. Marioni, Andrew N. J. McKenzie, Sarah A. Teichmann.

**Writing – review & editing:** Liora Haim-Vilmovsky, Johan Henriksson, Valentina Proserpio, Andrew N. J. McKenzie.

## References

1. Pulendran B, Artis D. New paradigms in type 2 immunity. *Science*. 2012; 337: 431–435. <https://doi.org/10.1126/science.1221064> PMID: 22837519
2. Halim TYF. Group 2 innate lymphoid cells in disease. *Int Immunol*. 2016; 28: 13–22. <https://doi.org/10.1093/intimm/dxv050> PMID: 26306498
3. Gasteiger G, Fan X, Dikiy S, Lee SY, Rudensky AY. Tissue residency of innate lymphoid cells in lymphoid and nonlymphoid organs. *Science*. 2015; 350: 981–985. <https://doi.org/10.1126/science.aac9593> PMID: 26472762
4. Jetten AM. Retinoid-related orphan receptors (RORs): critical roles in development, immunity, circadian rhythm, and cellular metabolism. *Nucl Recept Signal*. 2009; 7: e003. <https://doi.org/10.1621/nrs.07003> PMID: 19381306
5. Solt LA, Burriss TP. Action of RORs and their ligands in (patho)physiology. *Trends Endocrinol Metab*. 2012; 23: 619–627. <https://doi.org/10.1016/j.tem.2012.05.012> PMID: 22789990
6. Jetten AM, Kang HS, Takeda Y. Retinoic acid-related orphan receptors  $\alpha$  and  $\gamma$ : key regulators of lipid/glucose metabolism, inflammation, and insulin sensitivity. *Front Endocrinol*. 2013; 4: 1.
7. Cook DN, Kang HS, Jetten AM. Retinoic Acid-Related Orphan Receptors (RORs): Regulatory Functions in Immunity, Development, Circadian Rhythm, and Metabolism. *Nucl Receptor Res*. 2015; 2. <https://doi.org/10.11131/2015/101185> PMID: 26878025
8. Halim TYF, MacLaren A, Romanish MT, Gold MJ, McNagny KM, Takei F. Retinoic-acid-receptor-related orphan nuclear receptor alpha is required for natural helper cell development and allergic inflammation. *Immunity*. 2012; 37: 463–474. <https://doi.org/10.1016/j.immuni.2012.06.012> PMID: 22981535
9. Wong SH, Walker JA, Jolin HE, Drynan LF, Hams E, Camelo A, et al. Transcription factor ROR $\alpha$  is critical for nuocyte development. *Nat Immunol*. 2012; 13: 229–236. <https://doi.org/10.1038/ni.2208> PMID: 22267218
10. Lo BC, Gold MJ, Hughes MR, Antignano F, Valdez Y, Zaph C, et al. The orphan nuclear receptor ROR $\alpha$  and group 3 innate lymphoid cells drive fibrosis in a mouse model of Crohn's disease. *Sci Immunol*. 2016; 1: eaaf8864.
11. Han Y-H, Kim H-J, Na H, Nam M-W, Kim J-Y, Kim J-S, et al. ROR $\alpha$  Induces KLF4-Mediated M2 Polarization in the Liver Macrophages that Protect against Nonalcoholic Steatohepatitis. *Cell Rep*. 2017; 20: 124–135. <https://doi.org/10.1016/j.celrep.2017.06.017> PMID: 28683306
12. Yang XO, Pappu BP, Nurieva R, Akimzhanov A, Kang HS, Chung Y, et al. T helper 17 lineage differentiation is programmed by orphan nuclear receptors ROR alpha and ROR gamma. *Immunity*. 2008; 28: 29–39. <https://doi.org/10.1016/j.immuni.2007.11.016> PMID: 18164222
13. Malhotra N, Leyva-Castillo JM, Jadhav U, Barreiro O, Kam C, O'Neill NK, et al. ROR $\alpha$ -expressing T regulatory cells restrain allergic skin inflammation. *Sci Immunol*. 2018; 3. <https://doi.org/10.1126/sciimmunol.aao6923> PMID: 29500225
14. Walker JA, Clark PA, Crisp A, Barlow JL, Szeto A, Ferreira ACF, et al. Polychromic Reporter Mice Reveal Unappreciated Innate Lymphoid Cell Progenitor Heterogeneity and Elusive ILC3 Progenitors in Bone Marrow. *Immunity*. 2019; 51: 104–118.e7. <https://doi.org/10.1016/j.immuni.2019.05.002> PMID: 31128961

15. Henriksson J, Chen X, Gomes T, Ullah U, Meyer KB, Miragaia R, et al. Genome-wide CRISPR Screens in T Helper Cells Reveal Pervasive Crosstalk between Activation and Differentiation. *Cell*. 2019; 176: 882–896.e18. <https://doi.org/10.1016/j.cell.2018.11.044> PMID: 30639098
16. Love MI, Huber W, Anders S. Moderated estimation of fold change and dispersion for RNA-seq data with DESeq2. *Genome Biol*. 2014; 15: 550. <https://doi.org/10.1186/s13059-014-0550-8> PMID: 25516281
17. Weigmann B, Tubbe I, Seidel D, Nicolaev A, Becker C, Neurath MF. Isolation and subsequent analysis of murine lamina propria mononuclear cells from colonic tissue. *Nat Protoc*. 2007; 2: 2307–2311. <https://doi.org/10.1038/nprot.2007.315> PMID: 17947970
18. Tucker MS, Karunaratne LB, Lewis FA, Freitas TC, Liang Y-S. Schistosomiasis. *Curr Protoc Immunol*. 2001; Chapter 19: Unit 19.1.
19. Mann VH, Morales ME, Rinaldi G, Brindley PJ. Culture for genetic manipulation of developmental stages of *Schistosoma mansoni*. *Parasitology*. 2010; 137: 451–462. <https://doi.org/10.1017/S0031182009991211> PMID: 19765348
20. Pau G, Fuchs F, Sklyar O, Boutros M, Huber W. EBImage—an R package for image processing with applications to cellular phenotypes. *Bioinformatics*. 2010; 26: 979–981. <https://doi.org/10.1093/bioinformatics/btq046> PMID: 20338898
21. Bray NL, Pimentel H, Melsted P, Pachter L. Near-optimal probabilistic RNA-seq quantification. *Nat Biotechnol*. 2016; 34: 525–527. <https://doi.org/10.1038/nbt.3519> PMID: 27043002
22. Benaglia T, Chauveau D, Hunter D, Young D. mixtools: An R package for analyzing finite mixture models. *J Stat Softw*. 2009; 32: 1–29.
23. Patro R, Duggal G, Love MI, Irizarry RA, Kingsford C. Salmon provides fast and bias-aware quantification of transcript expression. *Nat Methods*. 2017. <https://doi.org/10.1038/nmeth.4197> PMID: 28263959
24. McCarthy DJ, Campbell KR, Lun ATL, Wills QF. Scater: pre-processing, quality control, normalization and visualization of single-cell RNA-seq data in R. *Bioinformatics*. 2017; 33: 1179–1186. <https://doi.org/10.1093/bioinformatics/btw777> PMID: 28088763
25. Picelli S, Faridani OR, Björklund ÅK, Winberg G, Sagasser S, Sandberg R. Full-length RNA-seq from single cells using Smart-seq2. *Nat Protoc*. 2014; 9: 171–181. <https://doi.org/10.1038/nprot.2014.006> PMID: 24385147
26. Butler A, Satija R. Integrated analysis of single cell transcriptomic data across conditions, technologies, and species. *bioRxiv*. 2017. Available: <https://www.biorxiv.org/content/early/2017/07/18/164889.abstract>
27. Stubbington MJT, Lönnberg T, Proserpio V, Clare S, Speak AO, Dougan G, et al. T cell fate and clonality inference from single-cell transcriptomes. *Nat Methods*. 2016; 13: 329–332. <https://doi.org/10.1038/nmeth.3800> PMID: 26950746
28. Bürglin TR, Henriksson J. FACSAnadu: Graphical user interface for rapid visualization and quantification of flow cytometry data. *bioRxiv*. 2017. p. 201897. <https://doi.org/10.1101/201897>
29. Folch J, Lees M, Sloane Stanley GH. A simple method for the isolation and purification of total lipides from animal tissues. *J Biol Chem*. 1957; 226: 497–509. PMID: 13428781
30. Ritchie ME, Phipson B, Wu D, Hu Y, Law CW, Shi W, et al. limma powers differential expression analyses for RNA-sequencing and microarray studies. *Nucleic Acids Res*. 2015; 43: e47. <https://doi.org/10.1093/nar/gkv007> PMID: 25605792
31. Stubbington MJT, Mahata B, Svensson V, Deonaraine A, Nissen JK, Betz AG, et al. An atlas of mouse CD4+ T cell transcriptomes. *Biol Direct*. 2015; 10: 14. <https://doi.org/10.1186/s13062-015-0045-x> PMID: 25886751
32. Lönnberg T, Svensson V, James KR, Fernandez-Ruiz D, Sebina I, Montandon R, et al. Single-cell RNA-seq and computational analysis using temporal mixture modelling resolves Th1/Tfh fate bifurcation in malaria. *Sci Immunol*. 2017; 2. <https://doi.org/10.1126/sciimmunol.aal2192> PMID: 28345074
33. Miragaia RJ, Gomes T, Chomka A, Jardine L, Riedel A, Hegazy AN, et al. Single-Cell Transcriptomics of Regulatory T Cells Reveals Trajectories of Tissue Adaptation. *Immunity*. 2019; 50: 493–504.e7. <https://doi.org/10.1016/j.immuni.2019.01.001> PMID: 30737144
34. Davidson S, Efremova M, Riedel A, Mahata B, Pramanik J, Huuhtanen J, et al. Single-cell RNA sequencing reveals a dynamic stromal niche within the evolving tumour microenvironment. *bioRxiv*. 2018. p. 467225. <https://doi.org/10.1101/467225>
35. Nemeth K, Keane-Myers A, Brown JM, Metcalfe DD, Gorham JD, Bundoc VG, et al. Bone marrow stromal cells use TGF- $\beta$  to suppress allergic responses in a mouse model of ragweed-induced asthma. *Proc Natl Acad Sci U S A*. 2010; 107: 5652–5657. <https://doi.org/10.1073/pnas.0910720107> PMID: 20231466

36. Moon JJ, Chu HH, Pepper M, McSorley SJ, Jameson SC, Kedl RM, et al. Naive CD4(+) T cell frequency varies for different epitopes and predicts repertoire diversity and response magnitude. *Immunity*. 2007; 27: 203–213. <https://doi.org/10.1016/j.immuni.2007.07.007> PMID: 17707129
37. Fang L, Adkins B, Deyev V, Podack ER. Essential role of TNF receptor superfamily 25 (TNFRSF25) in the development of allergic lung inflammation. *J Exp Med*. 2008; 205: 1037–1048. <https://doi.org/10.1084/jem.20072528> PMID: 18411341
38. Wang J, Fa J, Wang P, Jia X, Peng H, Chen J, et al. NINJ2- A novel regulator of endothelial inflammation and activation. *Cell Signal*. 2017; 35: 231–241. <https://doi.org/10.1016/j.cellsig.2017.04.011> PMID: 28431986
39. Castro G, Liu X, Ngo K, De Leon-Tabaldo A, Zhao S, Luna-Roman R, et al. ROR $\gamma$ t and ROR $\alpha$  signature genes in human Th17 cells. *PLoS One*. 2017; 12: e0181868. <https://doi.org/10.1371/journal.pone.0181868> PMID: 28763457
40. Miragaia RJ, Gomes T, Chomka A, Jardine L, Riedel A. Single cell transcriptomics of regulatory T cells reveals trajectories of tissue adaptation. *bioRxiv*. 2017. Available: <https://www.biorxiv.org/content/early/2017/11/22/217489.abstract>
41. Bollinger T, Leutz A, Leliavski A, Skrum L, Kovac J, Bonacina L, et al. Circadian clocks in mouse and human CD4+ T cells. *PLoS One*. 2011; 6: e29801. <https://doi.org/10.1371/journal.pone.0029801> PMID: 22216357
42. Akashi M, Takumi T. The orphan nuclear receptor ROR $\alpha$  regulates circadian transcription of the mammalian core-clock Bmal1. *Nat Struct Mol Biol*. 2005; 12: 441. <https://doi.org/10.1038/nsmb925> PMID: 15821743
43. Fei F, Qu J, Zhang M, Li Y, Zhang S. S100A4 in cancer progression and metastasis: A systematic review. *Oncotarget*. 2017; 8: 73219–73239. <https://doi.org/10.18632/oncotarget.18016> PMID: 29069865
44. Grum-Schwensen B, Klingelhöfer J, Beck M, Bonefeld CM, Hamerlik P, Guldborg P, et al. S100A4-neutralizing antibody suppresses spontaneous tumor progression, pre-metastatic niche formation and alters T-cell polarization balance. *BMC Cancer*. 2015; 15: 44. <https://doi.org/10.1186/s12885-015-1034-2> PMID: 25884510
45. Mandai Y, Takahashi D, Hase K, Ebisawa M, Nakagawa T, Sato T, et al. S1711 Distinct Roles for Cxcr6 and Cxcr6- CD4 T Cells in the Pathogenesis of Chronic Colitis. *Gastroenterology*. 2010; 138: S–258.
46. Latta M, Mohan K, Issekutz TB. CXCR6 is expressed on T cells in both T helper type 1 (Th1) inflammation and allergen-induced Th2 lung inflammation but is only a weak mediator of chemotaxis. *Immunology*. 2007; 121: 555–564. <https://doi.org/10.1111/j.1365-2567.2007.02603.x> PMID: 17437534
47. Bitsch F, Aichholz R, Kallen J, Geisse S, Fournier B, Schlaeppi JM. Identification of natural ligands of retinoic acid receptor-related orphan receptor alpha ligand-binding domain expressed in Sf9 cells—a mass spectrometry approach. *Anal Biochem*. 2003; 323: 139–149. <https://doi.org/10.1016/j.ab.2003.08.029> PMID: 14622968
48. Zhang Z, Burch PE, Cooney AJ, Lanz RB, Pereira FA, Wu J, et al. Genomic analysis of the nuclear receptor family: new insights into structure, regulation, and evolution from the rat genome. *Genome Res*. 2004; 14: 580–590. <https://doi.org/10.1101/gr.2160004> PMID: 15059999
49. Harnett W, Harnett MM, Byron O. Structural/functional aspects of ES-62—a secreted immunomodulatory phosphorylcholine-containing filarial nematode glycoprotein. *Curr Protein Pept Sci*. 2003; 4: 59–71. <https://doi.org/10.2174/1389203033380368> PMID: 12570785
50. Jung DE, Kim JM, Kim C, Song SY. Embigin is overexpressed in pancreatic ductal adenocarcinoma and regulates cell motility through epithelial to mesenchymal transition via the TGF- $\beta$  pathway. *Mol Carcinog*. 2016; 55: 633–645. <https://doi.org/10.1002/mc.22309> PMID: 25773908
51. Weaver CT, Hatton RD, Mangan PR, Harrington LE. IL-17 family cytokines and the expanding diversity of effector T cell lineages. *Annu Rev Immunol*. 2007; 25: 821–852. <https://doi.org/10.1146/annurev.immunol.25.022106.141557> PMID: 17201677
52. Yasuhara R, Irié T, Suzuki K, Sawada T, Miwa N, Sasaki A, et al. The  $\beta$ -catenin signaling pathway induces aggressive potential in breast cancer by up-regulating the chemokine CCL5. *Exp Cell Res*. 2015; 338: 22–31. <https://doi.org/10.1016/j.yexcr.2015.09.003> PMID: 26363360
53. Khaled AR, Durum SK. Lymphocyte: cytokines and the control of lymphoid homeostasis. *Nat Rev Immunol*. 2002; 2: 817–830. <https://doi.org/10.1038/nri931> PMID: 12415306
54. Lodolce JP, Boone DL, Chai S, Swain RE, Dassopoulos T, Trettin S, et al. IL-15 Receptor Maintains Lymphoid Homeostasis by Supporting Lymphocyte Homing and Proliferation. *Immunity*. 1998; 9: 669–676. [https://doi.org/10.1016/s1074-7613\(00\)80664-0](https://doi.org/10.1016/s1074-7613(00)80664-0) PMID: 9846488
55. Hunter CA, Jones SA. IL-6 as a keystone cytokine in health and disease. *Nat Immunol*. 2015; 16: 448–457. <https://doi.org/10.1038/ni.3153> PMID: 25898198

56. Peine M, Marek RM, Löhning M. IL-33 in T Cell Differentiation, Function, and Immune Homeostasis. *Trends Immunol.* 2016; 37: 321–333. <https://doi.org/10.1016/j.it.2016.03.007> PMID: 27055914
57. Liu Y, Cai Y, Liu L, Wu Y, Xiong X. Crucial biological functions of CCL7 in cancer. *PeerJ.* 2018; 6: e4928. <https://doi.org/10.7717/peerj.4928> PMID: 29915688
58. Qin X-J, Shi H-Z, Deng J-M, Liang Q-L, Jiang J, Ye Z-J. CCL22 recruits CD4-positive CD25-positive regulatory T cells into malignant pleural effusion. *Clin Cancer Res.* 2009; 15: 2231–2237. <https://doi.org/10.1158/1078-0432.CCR-08-2641> PMID: 19318474
59. Vulcano M, Albanesi C, Stoppacciaro A, Bagnati R, D'Amico G, Struyf S, et al. Dendritic cells as a major source of macrophage-derived chemokine/CCL22 in vitro and in vivo. *Eur J Immunol.* 2001; 31: 812–822. [https://doi.org/10.1002/1521-4141\(200103\)31:3<812::aid-immu812>3.0.co;2-I](https://doi.org/10.1002/1521-4141(200103)31:3<812::aid-immu812>3.0.co;2-I) PMID: 11241286
60. Campbell JJ, O'Connell DJ, Wurbel M-A. Cutting Edge: Chemokine receptor CCR4 is necessary for antigen-driven cutaneous accumulation of CD4 T cells under physiological conditions. *J Immunol.* 2007; 178: 3358–3362. <https://doi.org/10.4049/jimmunol.178.6.3358> PMID: 17339428
61. Arojo OA, Ouyang X, Liu D, Meng T, Kaech SM, Pereira JP, et al. Active mTORC2 Signaling in Naive T Cells Suppresses Bone Marrow Homing by Inhibiting CXCR4 Expression. *J Immunol.* 2018. <https://doi.org/10.4049/jimmunol.1800529> PMID: 29934471
62. Halim TYF, Steer CA, Mathä L, Gold MJ, Martinez-Gonzalez I, McNagny KM, et al. Group 2 innate lymphoid cells are critical for the initiation of adaptive T helper 2 cell-mediated allergic lung inflammation. *Immunity.* 2014; 40: 425–435. <https://doi.org/10.1016/j.immuni.2014.01.011> PMID: 24613091
63. He W, Holtkamp S, Hergenhan SM, Kraus K, de Juan A, Weber J, et al. Circadian Expression of Migratory Factors Establishes Lineage-Specific Signatures that Guide the Homing of Leukocyte Subsets to Tissues. *Immunity.* 2018. <https://doi.org/10.1016/j.immuni.2018.10.007> PMID: 30527911
64. Druz D, Matveeva O, Ince L, Harrison U, He W, Schmal C, et al. Lymphocyte Circadian Clocks Control Lymph Node Trafficking and Adaptive Immune Responses. *Immunity.* 2017; 46: 120–132. <https://doi.org/10.1016/j.immuni.2016.12.011> PMID: 28087238
65. Kim K, Boo K, Yu YS, Oh SK, Kim H, Jeon Y, et al. ROR $\alpha$  controls hepatic lipid homeostasis via negative regulation of PPAR $\gamma$  transcriptional network. *Nat Commun.* 2017; 8: 162. <https://doi.org/10.1038/s41467-017-00215-1> PMID: 28757615
66. Li M, Ransohoff RM. Multiple roles of chemokine CXCL12 in the central nervous system: a migration from immunology to neurobiology. *Prog Neurobiol.* 2008; 84: 116–131. <https://doi.org/10.1016/j.pneurobio.2007.11.003> PMID: 18177992